Kinematic behavior of southern Alaska constrained by westward decreasing postglacial slip rates on the Denali Fault, Alaska

A.-S. Mériaux,[1,2] K. Sieh,[3] R. C. Finkel,[1,4] C. M. Rubin,[5] M. H. Taylor,[3,6] A. J. Meltzner,[3] and F. J. Ryerson[1]

Received 16 March 2007; revised 3 November 2008; accepted 9 December 2008; published 12 March 2009.

[1] Long-term slip rates for the Denali Fault in southern Alaska are derived using ^{10}Be cosmogenic radionuclide (CRN) dating of offset glacial moraines at two sites. Correction of ^{10}Be CRN model ages for the effect of snow shielding uses historical, regional snow cover data scaled to the site altitudes. To integrate the time variation of snow cover, we included the relative changes in effective wetness over the last 11 ka, derived from lake-level records and δ^{18}O variations from Alaskan lakes. The moraine CRN model ages are normally distributed around an average of 12.1 ± 1.0 ka (n = 22, ± 1σ). The slip rate decreases westward from ~13 mm/a at 144°49′W to about 7 mm/a at 149°26′W. The data are consistent with a kinematic model in which southern Alaska translates northwestward at a rate of ~14 mm/a relative to a stable northern Alaska with no rotation. This suggests progressive slip partitioning between the Denali Fault and the active fold and thrust belt at the northern front of the Alaska range, with convergence rates increasing westward from ~4 mm/a to 11 mm/a between ~149°W and 145°W. As the two moraines sampled for this study were emplaced synchronously, our suggestion of a westward decrease in the slip rate of the Denali Fault relies largely upon the measured offsets at both sites, regardless of any potential systematic uncertainty in the CRN model ages.

Citation: Mériaux, A.-S., K. Sieh, R. C. Finkel, C. M. Rubin, M. H. Taylor, A. J. Meltzner, and F. J. Ryerson (2009), Kinematic behavior of southern Alaska constrained by westward decreasing postglacial slip rates on the Denali Fault, Alaska, *J. Geophys. Res.*, *114*, B03404, doi:10.1029/2007JB005053.

1. Introduction

[2] The right-lateral strike-slip Denali Fault is a major element in the complex northern boundary between the North American and Pacific plates [*St. Amand*, 1957]. Although the principal element in the plate boundary is the Alaskan-Aleutian megathrust, other active continental structures lie to the north (Figure 1). One of these is the Denali Fault, a dextral ~2000-km-long strike-slip structure that traverses the rugged Alaska Range of south central Alaska for about 780 km. The crustal block south of the Denali Fault is called the Wrangell block, as defined by *Lahr and Plafker* [1980]. Two end-member tectonic models can be invoked to explain the intracontinental deformation of southern Alaska and the growth of the Alaska Range. The spatial variation in millennial slip along the Denali Fault plays an important role in testing the plausibility of these models. At one extreme, a kinematic model, suggested by the arcuate geometry of the Denali Fault, in which the Wrangell block rotates counterclockwise relative to North America [*St. Amand*, 1957; *Stout and Chase*, 1980; *Lahr and Plafker*, 1980; *Page et al.*, 1995], requires neither along-strike variation in the lateral slip rate nor deformation north of the Denali Fault. Consequently, slip along the Denali Fault and shortening across the Alaska Range are decoupled. Alternatively, northwestward translation of the Wrangell block with respect to the North American plate without significant counterclockwise, vertical-axis rotation requires a westward decrease in the lateral slip rate. In this case, convergence rates across the Alaska Range's northern frontal thrust fault system would increase from east to west as increasing fault slip is transferred from the Denali Fault to thrust systems.

[3] One might see support for the second model in the decidedly asymmetric distribution of slip along the Denali Fault during the Mw 7.9 2002 earthquake [*Eberhart-Phillips et al.*, 2003; *Haeussler et al.*, 2004], if this event was characteristic of the long-term behavior of the Denali Fault. The distribution of dextral slip along the 220-km rupture during this earthquake decreases from about 9 m in the east to about 3 m in the west [*Eberhart-Phillips et al.*, 2003; *Hreinsdottir et*

[1]Institute of Geophysics and Planetary Physics, Lawrence Livermore National Laboratory, Livermore, California, USA.
[2]Now at School of Geography, Politics and Sociology, University of Newcastle, Newcastle Upon Tyne, UK.
[3]Division of Geologic and Planetary Science, California Institute of Technology, Pasadena, California, USA.
[4]Now at Earth and Planetary Science Department, University of California, Berkeley, California, USA.
[5]Department of Geological Sciences, Central Washington University, Ellensburg, Washington, USA.
[6]Now at Department of Geology, University of Kansas, Lawrence, Kansas, USA.

0148-0227/09/2007JB005053$09.00

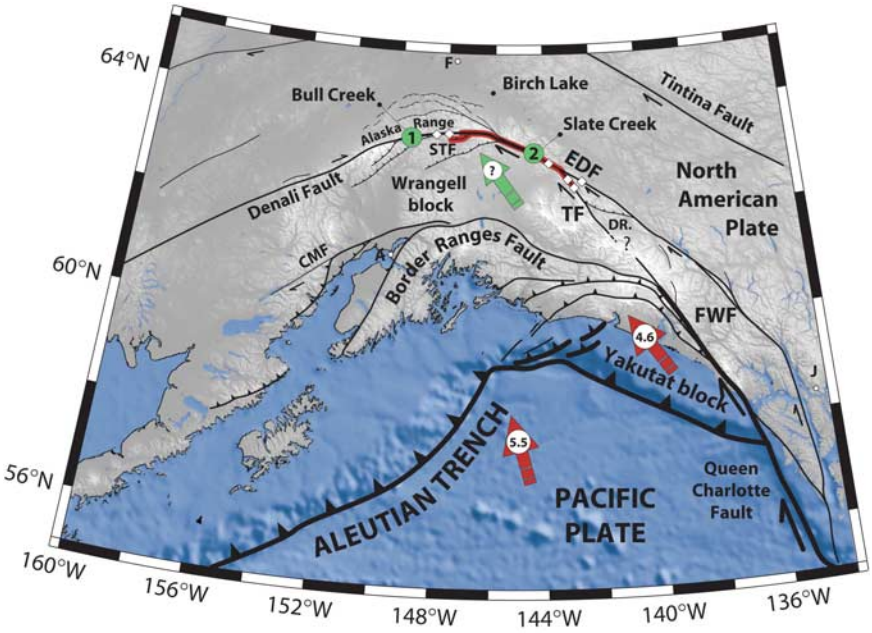

Figure 1. Tectonic map of southern Alaska with major faults forming Pacific–North American plate boundary. Convergence rates of North Pacific plates and Yakutat block are indicated with red arrows [*DeMets and Dixon*, 1999]. Rupture for the 2002 November Mw7.9 Denali Fault earthquake is outlined by thick red line [*Eberhart-Phillips et al.*, 2003]. EDF, Eastern Denali Fault; FWF, Fairweather Fault; TF, Totschunda Fault; DRF, Duke River Fault; STF, Sustina Glacier Fault; CMF, Castle Mountain Fault. Sites of this study are located in green circles; 1, Bull Creek site; 2, Slate Creek site. White diamonds are site locations of *Matmon et al.* [2006]. Cities of Juneau (J), Anchorage (A), and Fairbanks (F) are indicated as well as Birch Lake.

al., 2003; *Wright et al.*, 2004; *Haeussler et al.*, 2004]. Here we investigate whether the long-term slip rate on the Denali Fault might likewise decrease westward, as suggested by the results of *Matmon et al.* [2006]. If verified, this correlation would support a model in which the distribution of co-seismic slip during the 2002 quake is characteristic of the fault's long-term behavior. The apparent westward decrease of total right-lateral slip along the Denali Fault, from 400 to 350 km on the eastern segment to ~100 km on the McKinley strand of the fault system [cf. *Plafker and Berg*, 1994], also lends supports to the second model and further links the distribution of co-seismic slip to the long-term growth of topography.

[4] Determining the long-term slip rate of the Denali Fault by averaging over numerous seismic cycles should enable testing of these two models. Until recently, however, determination of slip rates from offset landforms along the Denali Fault was hampered by the lack of reliable geochronologic constraints. All slip rate estimates assumed climatic correlations to approximate the age of offset features such as moraines and periglacial fans. These studies yielded slip rates that range between 10 and 20 mm/a [*Richter and Matson*, 1971; *Stout et al.*, 1973; *Hickman et al.*, 1977; *Sieh*, 1981] but did not have sufficient precision to constrain spatial variations in the slip rate.

[5] The development of surface exposure age dating using in situ cosmogenic nuclides has improved our ability to directly date morphological features, such as periglacial fans and moraines [i.e., *Nishiizumi et al.*, 1989; *Gosse et al.*, 1995a, 1995b; *Stone*, 2000; *Gosse and Phillips*, 2001] and has made fault slip rate estimates in glaciated areas possible, extending the geomorphic observation interval beyond that accessible to radiocarbon dating [*Van der Woerd et al.*, 1998; *Lasserre et al.*, 2002; *Brown et al.*, 2002; *Mériaux et al.*, 2004a; *Chevalier et al.*, 2005]. In this study, dextrally offset moraines were sampled for ^{10}Be CRN dating at two sites along the Denali Fault, ~235 km apart, to estimate the average slip rates.

[6] A similar study by *Matmon et al.* [2006] recently estimated slip rates using CRN surface exposure dating to constrain offset markers at four sites along the arcuate section of Denali Fault and at three additional sites on Totschunda Fault (TF) and Eastern Denali Fault (EDF). The two studies were conducted simultaneously and independently after the 2002 Denali Fault earthquake. *Matmon et al.* [2006] estimated average slip rates of 9.4 ± 1.6, 12.1 ± 1.7, and 8.4 ± 2.2 mm/a along the western, central, and eastern Denali Fault, respectively. Based upon the rates for the central and western Denali Faults, *Matmon et al.* [2006] suggested that the slip rate may be decreasing to the west. Note that the rate on the eastern Denali Fault (EDF) is not directly relevant here as the slip on the Denali Fault is partitioned between the TF and the EDF east of the junction between the 2 strike-slip faults. However, the rate estimates on the Denali Fault are indistinguishable within error, and further measurements on sites to the west of those sampled by *Matmon et al.* [2006] are required to verify this trend. In this connection we report rates from two sites on the central Denali Fault: (1) an eastern site, Slate Creek, which had also been sampled by *Matmon et al.* [2006] is located on the main strand of the Denali Fault at

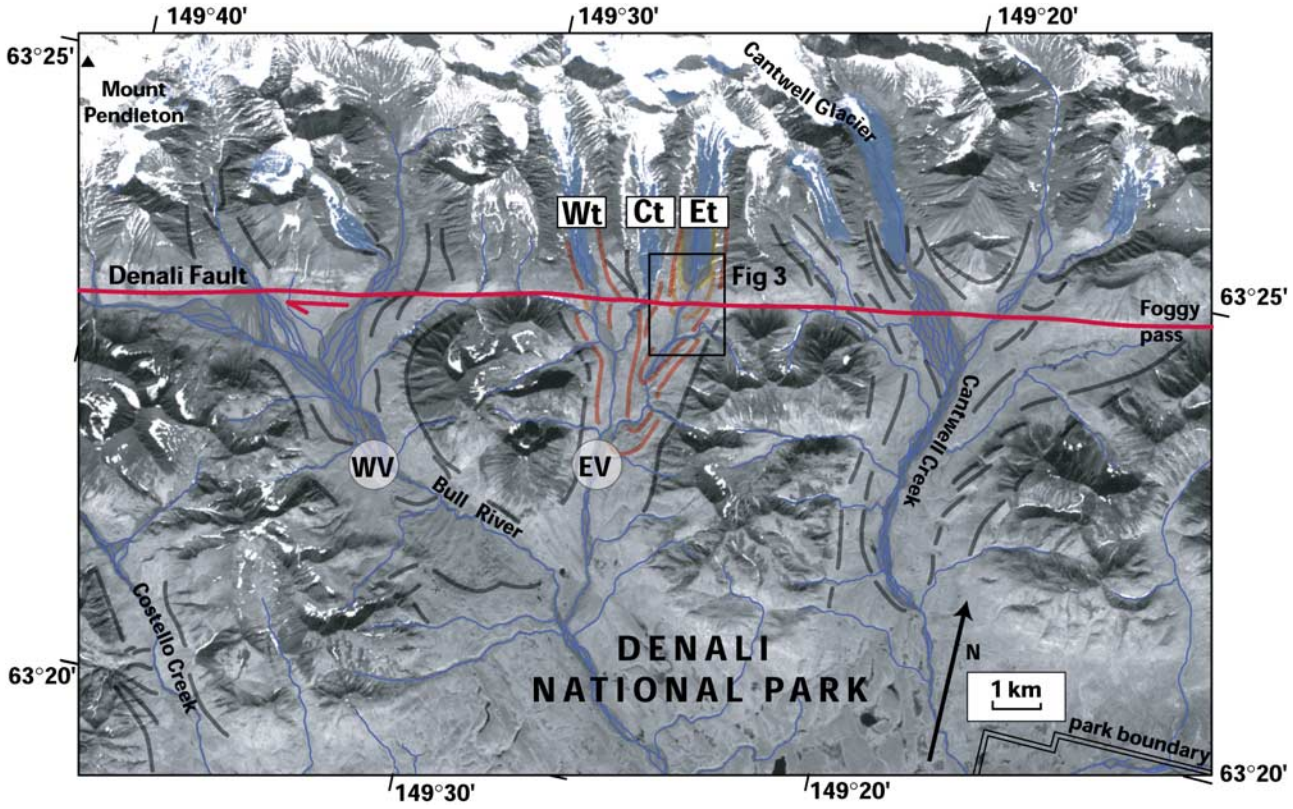

Figure 2. Orthorectified Landsat image of the Bull Creek area in the SE corner of the Denali National Park. Glaciers are colored in blue together with river and streams. Bull Creek valley comprises the eastern (EV) and western valleys (WV). Undifferentiated moraines are mapped in gray lines. Moraines at Bull Creek site are mapped with relative age constrain as indicated by colors line (red represents older; orange represents intermediate; yellow represents young). Wt, Ct, and Et are western, central, and eastern tributaries. Box outlines area of Figure 3.

~144°49′W, ~78 km northwest of the Mentasta pass junction and ~60 km southeast of the Delta River junction (this portion of the fault ruptured during the 2002 Mw 7.9 Denali earthquake, Figure 1) and (2) a western site, at Bull Creek, located in the Denali National Park at ~149°26′W on the McKinley strand of the Denali Fault (this segment did not rupture in 2002, Figure 1). This site is located ~50 km west of the westernmost site of *Matmon et al.* [2006]. At both sites we targeted well-preserved younger moraines that preserve clear dextral offsets.

2. Geomorphic Offsets Along the Denali Fault

[7] Along the trace of the Denali Fault are numerous stream channels, drainages and ridges that display offsets ranging from a few meters to a few kilometers [*Richter and Matson*, 1971; *Stout et al.*, 1973; *Hickman et al.*, 1977; *Sieh*, 1981; *Matmon et al.*, 2006]. Determining a long-term slip rate based on such offset features remains a challenge, however, because the offset features must be both well defined and datable. Unfortunately, the clear and common stream-related offsets are difficult to date, as they are typically refreshed by stream action. This factor alone drastically reduces the number of offsets useful in establishing slip rate estimates. Although, the preserved landforms should be datable by radiocarbon dating as most of them postdate the Last Glacial Maximum that clearly overprinted the morphology of the Alaskan Range. The deposition and preservation of carbon in these commonly coarse deposits is uncommon and difficult to access. Hence, CRN dating of geomorphic features is a more practical geochronologic method. Here, we present morphochronologic data from the Bull Creek and Slate Creek sites where we have been able to date the abandonment ages of well-defined offset glacial moraines and thereby determine slip rates.

2.1. Offset Moraine at the Bull Creek Site

[8] The Bull Creek site lies along the N80°E striking McKinley strand of the Denali Fault, at ~149°26′W and ~1050 m elevation, flanking the southern face of the Alaska Range (Figure 1). Bull Creek River is a south-flowing braided tributary of West Fork River and originates in some of the higher peaks of the southeastern corner of the Mount McKinley massif. Bull Creek valley is divided into a western valley (WV) and an eastern valley (EV), each of which originates from small catchments whose surrounding peaks reach altitudes of ~2150 m (Figure 2). The sampling site is located within the easternmost of three tributaries (Et, Figure 2) of the eastern valley, a few hundred meters downstream from a minor (~370-m-wide) unnamed modern glacier (Figure 2).

[9] The active trace of the Denali Fault is particularly clear in this region (Figures 2 and 3). This portion of the

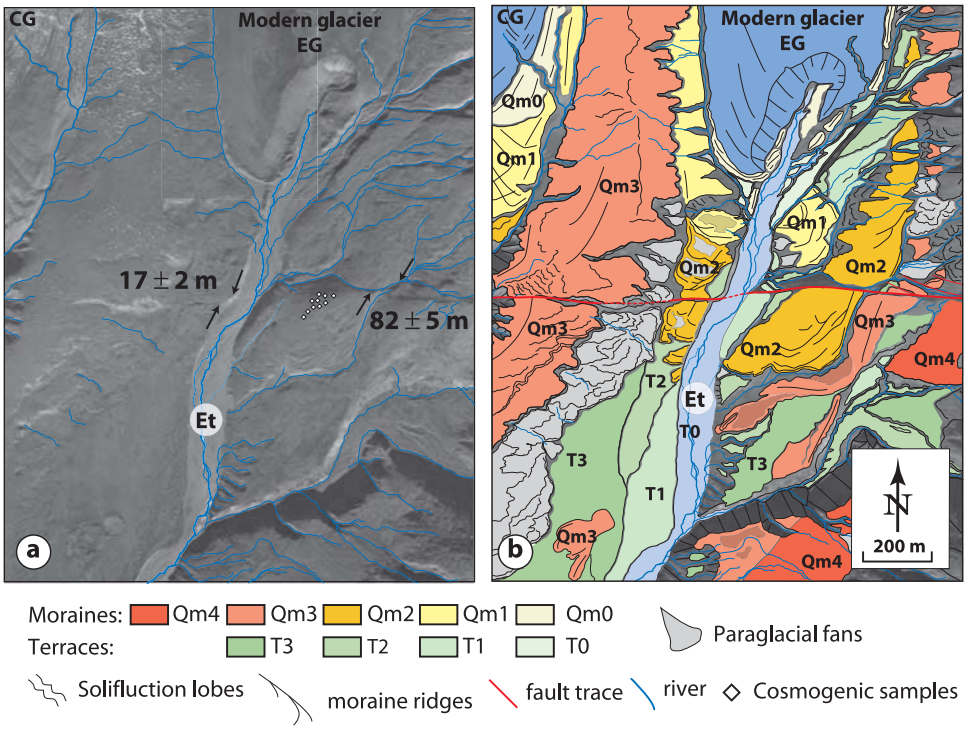

Figure 3. (a) 1973 vertical aerial photograph with CRN sample locations in white diamonds. Offsets are indicated with black arrows. Note offsets of Qm2 (82 ± 5m) and western riverbank of the eastern tributary (Et, 17 ± 2 m). (b) Geomorphic interpretation of the inset moraines at Bull Creek site. Relative age of Quaternary moraines (Qm) is indicated with color and increase numbering from younger (Qm0) to older (Qm4). CG and EG are central and eastern glaciers, respectively.

fault is characterized by numerous right-lateral offsets ranging from about ten meters to a few hundred meters [*Hickman et al.*, 1977; *Sieh*, 1981]. Of the three tributaries of the eastern valley, only the central and the eastern tributaries (Ct and Et, Figure 2) flow roughly perpendicular to the Denali Fault. The fault deflects them right-laterally by amounts that we estimate to be ~273 m and ~266 m, respectively (Figures 2 and 3). A fluvial terrace riser, T1-Qm2/T0, on the west bank of the eastern tributary is offset 17 ± 2 m, based on our measurement made using a total station (Figure 3). This measurement agrees with previous estimates of 15 m, made on vertical aerial photos taken in 1973 [*Sieh*, 1981].

[10] Four sets of inset moraines exist at the Bull Creek site (Figure 3). The highest and oldest moraine, Qm4, appears only on the eastern side of the valley. A lower and younger set of moraines, Qm3, is the most extensive in the valley and is well preserved, especially south of the fault. The Qm3 moraines comprise recessional and terminal moraines that extend ~1.8–3.3 km from the front of the modern glacial terminus (Figure 2). Three sets of well-defined fluvial terraces formed in the valley since the abandonment and breaching of these Qm3 moraines (T3, T2, and T1, Figure 3) indicating several aggradation periods of Et since that time. The recessional and terminal Qm3 moraines extend downstream from the fault, whereas the lateral and medial moraines extend upstream to the edge of the modern glacier, mostly north of the fault (Figure 3). Unfortunately, erosion of these lateral moraines is so severe, especially near the fault trace, that they yield only rough estimates of their dextral offset, with large uncertainties. Thus, we did not sample the Qm3 moraines for CRN exposure dating.

[11] A still younger set of lateral and terminal moraines, Qm2, exists on both sides of the valley, and overrode fluvial terrace T2. The active riverbed has entrenched the Qm2 moraines. Qm2 extends about 225 m south of the fault trace and ~580 m from the terminus of the modern glacier (Figure 3). The left- and right-lateral moraines are not symmetrical; the left-lateral (eastern) Qm2 moraines are well defined and strike roughly perpendicular to the fault trace, but the right-lateral (western) Qm2 moraines are more complex. They consist of small, discontinuous lateral moraines and a chaotic pile of large terminal moraines located both upstream and downstream from the fault (Figure 3). The asymmetry of the Qm2 moraines resembles the geometry of the youngest moraine (Qm0), located upstream, nearer the modern glacier. Similarly, the peculiar setting of Qm0 seems to reflect the asymmetry of the modern glacial terminus; the river outlet emerging from the glacial terminus is east of the glaciers medial line and so the eastern half of the glacial tongue is more melted than the western side. The asymmetry of the ice is mimicked in the moraine geometries. By analogy, we interpret the asymmetry of the Qm2 moraines to have a similar origin. This implies that at a given location along the river, the left-bank ice retreat occurs earlier than on the western side, leaving a slightly older eastern lateral moraine downstream.

[12] The clearest offset feature within Qm2 is a narrow moraine crest on the eastern flank of the moraine complex. To gain a precise measurement of the offset, we prepared a

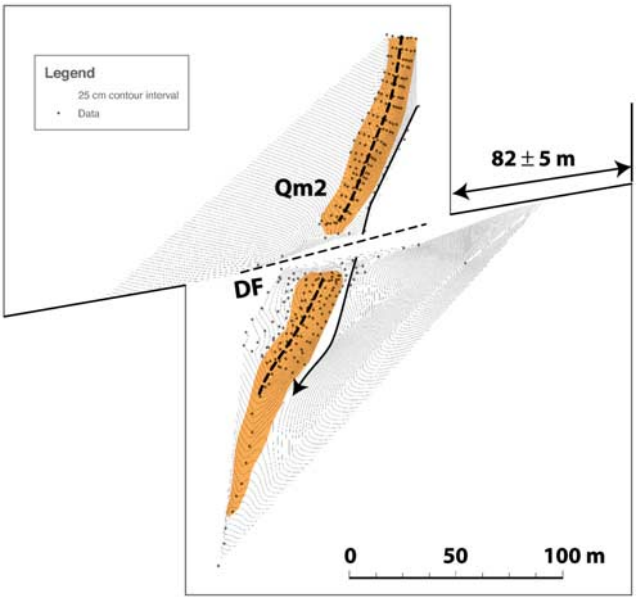

Figure 4. Retrodeformation of Offset at Bull Creek as deduced from total station map around well-defined Qm2 crest and marginal ice channel. Dots correspond to the grounds control points leveled for the map. Dash line corresponds to moraine crest. Line with arrow represents the marginal ice channel.

map of that crest using a total station. The moraine crest strikes roughly perpendicular to the fault and is dextrally offset 82 ± 5 m (Figures 3 and 4), as is the marginal ice channel immediately east of the crest (Figure 4). We collected samples for CRN exposure dating from the most gently dipping Qm2 surface, south of the fault trace and near the offset moraine and ice-marginal channel (Figure 3a).

[13] The offset of the western margin of the Qm2 moraine set is not as well defined as the eastern margin. Its offset is approximately 60 m. A 25% smaller offset of the western flank of the Qm2 moraines due solely to the diachronous abandonment of the moraine resulting from asymmetry of the glacier retreat seems rather large. This would suggest a younger age for the western Qm2 flank of up to 25%, which is highly unlikely considering the relative high velocity of glacier retreat in general. Given the greater ambiguity of this measurement, however, it seems appropriate to take it rather as a minimum bound for Qm2 offset.

2.2. Offset Moraine at the Slate Creek Site

[14] The Slate Creek site is ~235 km east of the Bull Creek site, at an elevation of ~1320 m (Figure 1). Slate Creek, the principal local drainage, flows from terminus of the western tongue of the hammerhead-shaped Chistochina glacier (Figure 5). The Denali Fault runs N59°W across the site.

[15] Earlier glacial advances of three south-flowing glaciers (WG, CG, and EG) associated with the western tongue of the Chistochina glacier have left glacial landforms and deposits that cross the fault trace at high angles and are tectonically offset (Figures 5 and 6). We refer to three braided tributaries emanating from these valleys as the eastern (Et), central (Ct), and western tributaries (Wt); these in turn merge to form Slate Creek. The confluence of the western and central tributaries is about 360 m south of the Denali Fault, and their confluence with the eastern tributary is about 1 km further south. The studied offsets are located between the central and eastern tributaries (Figure 6). Coseismic offsets associated with the 2002 earthquake ranged from 4.70 to 5.32 m in this area (138.88–151.4.457 km) [*Haeussler et al.*, 2004, Figure 5]. Between Wt and Et, *Haeussler et al.* [2004] measured the horizontal slip of four markers solely on the main trace of the rupture of the 2002 quake (Figure 5). However, detailed mapping of the rupture based on field observations and postearthquake aerial photo interpretation indicates a rather wide fault zone extending up to about 140 m to the north, perpendicular to the main trace, between Ct and Wt with a complex slip distribution among numerous strands (Figures 7 and 8 and auxiliary material).[1] Thus, the mean value of 5.0 ± 0.3 m (±1σ) derived from *Haeussler et al.* [2004] must be considered as a minimum bound for the effective coseismic slip at Slate Creek.

[16] The confluence of the western, central and eastern moraines at the Slate Creek site has produced a more complex depositional history and geometry than that at Bull Creek. The youngest terminal moraines (Qm0), near the modern glaciers and largely associated with the main body of the Chistochina glacier, are confined to three individual steep-walled glacial canyons and do not cross the fault (Figures 5 and 6). An older set of moraines (Qm1) extends farther south but also not across the fault (Figures 5–7). A still older group of moraines (Qm2) extends out onto the plain south of the three tributaries and across the Denali Fault (Figures 5–7). The fault has clearly offset a number of Qm2 moraine ridges and swales on the eastern flank of this group.

[17] Lateral and medial moraines, paraglacial sedimentation (e.g., kame terraces), and secondary fans are inlaid between the moraine ridges. The western ~215-m-wide Qm2 bench, located in between the western and the central outwash, is well expressed about 85 m north of the main fault trace (Figure 7). No evidence of this Qm2 bench can be mapped on the south side of the fault, west of the Ct. The central ~300-m-wide bench, located east of the Ct, is limited on its eastern side by a NW–SE-trending lateral meltwater channel (c2, Figures 6 and 7). This bench is dissected near its center by another meltwater channel, c1, which roughly parallels c2 and is subperpendicular to the fault on its north side. As c1 approaches the fault traces, it becomes progressively dextrally deflected as it crosses each of the secondary faults and then follows the main fault trace, before merging with Ct to the west (Figures 6 and 7). A moraine bench and adjacent meltwater channels (c1′, c2′) with similar surface characteristics and geometry are also observed south of the main fault. Because the surface roughness and geometry of the bench and meltwater channels is similar, we conclude that they were once the same moraine that has been cut and displaced by the Denali Fault. To estimate the cumulative offset of Qm2, we quantified the various displacements along the numerous fault strands within the ~140 m wide fault zone (Figure 7). On the main trace, the retrodeformation of the moraines ridges and valleys between Et and c2 implies an offset of 122 ± 5 m, to which must be added the offset on the minors faults, f1,

[1] Auxiliary materials are available in the HTML. doi:10.1029/2007JB005053.

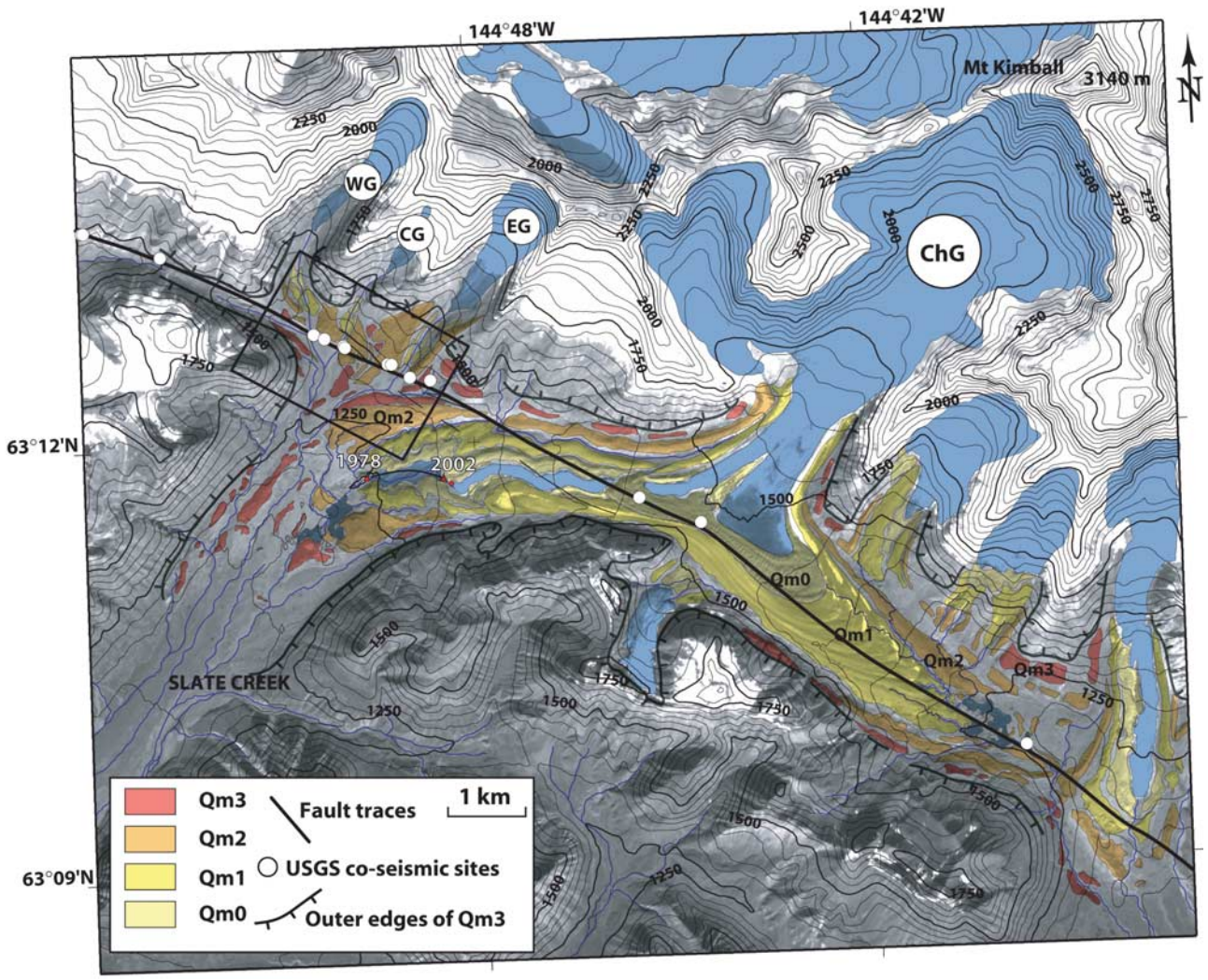

Figure 5. Small-scale regional map of the Chistochina glacial area, using a preearthquake SPOT image (10 m resolution) with overlapping DEM contour lines from the National Elevation Data set (∼90 m resolution). Relative age of Quaternary moraines (Qm) is indicated with color and increase numbering from younger (Qm0) to older (Qm4). Glaciers and hydraulic network are outlined in blue. White circles are site locations of *Haeussler et al.* [2004]. Note the small red circles indicating the ice retreat between 1973 and 2002. ChG is the Chistichina glacier. WG, CG, and EG are western glacier, central glacier, and eastern glacier, respectively. Box outlines area of Figure 6.

f2, f3, and f4 (Figure 7). The offset uncertainty on the main branch is based on the width of the meltwater channels as measured from the high-resolution aerial photograph (Figure 7). The cumulative slip component of the secondary faults is mostly strike slip together with a normal component of about 1/4 of the horizontal slip (Figure 8a). The cumulative offset estimates measured on these faults, derived from the retrodeformations that followed the detailed mapping of the fault zone, range from 6 to 19 m (Figure 7). Overall, the dextral offset is estimated to be 166 ± 25 m at this site, with the offset uncertainty based on the two end-member retrodeformation models (Figure 7). Here, the cumulative contribution of the secondary faults appears to be ∼27% of the total deformation. If this contribution remains somewhat constant over time, the coseismic value of *Haeussler et al.* [2004] is similarly underestimated by ∼27%. This would imply a local coseismic slip for the 2002 quake to be 6.8 ± 1.0 m at Slate Creek, which is comparable with the higher values found east and west of this site by *Haeussler et al.* [2004]. Moreover, *Taylor et al.* [2008] measured a maximum coseismic horizontal slip to be 7.5 ± 1.12 m, using subpixel cross correlation of SPOT images at Slate Creek. This would imply an even larger contribution of the secondary faults for the last event of up to 33% and would yield a maximum cumulative offset of 183 ± 30 m for Qm2. In both latter cases, we assume that the coseismic slip during the 2002 quake is characteristic of the fault's long-term behavior, not only on the main trace of the fault but also on the secondary faults. The ''true offset'' of Qm2 measured here must be larger than that determined by *Matmon et al.* [2006] as they did not include the cumulative secondary fault displacements. However, concatenation of the errors associated with the cumulative offset does not yield a result that is statistically distinct from their 144 ± 14 m

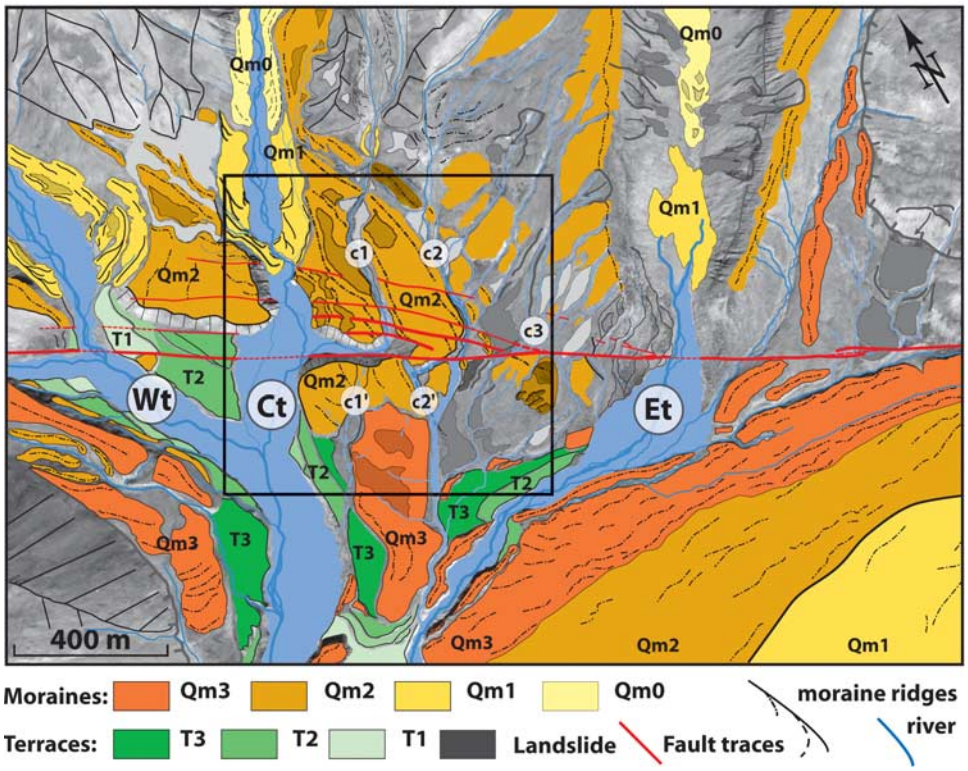

Figure 6. Regional map at Slate Creek using the 1973 aerial photo. Quaternary moraines (Qm) are indicated with colors and increase numbering from younger (Qm0) to older (Qm3). Inset paraglacial sedimentations of moraines have the same color code but are opaque. Ridges are dark lines. Wt, Ct, and Et are western, central, and eastern tributaries, respectively. C1 and C2 are channel 1 and 2, upstream from fault; counterpart channels downstream are C1′ and C2′, respectively. Arrows indicate the direction of land sliding. Box outlines area of Figure 7.

offset estimate. As at Bull Creek, Qm2 is best preserved and was sampled for CRN exposure dating on both sides of the main fault trace (Figure 7a).

3. Cosmogenic Dating of Offset Glacial Moraines

3.1. The ^{10}Be Surface Exposure Dating

[18] Surface exposure dating using in situ produced CRN such as ^{10}Be can be used to date moraines with a precision of up to ~4% [e.g., *Nishiizumi et al.*, 1989; *Gosse et al.*, 1995a, 1995b]. Assuming no preexposure, the exposure age of a sample is given by [*Lal*, 1991]:

$$t(z) = \frac{-1}{\lambda + \mu\varepsilon} \ln\left(1 - \frac{N(\lambda + \rho\varepsilon/\Lambda)e^{\mu z}}{C_s P_0}\right), \qquad \text{with } \mu = \frac{\rho}{\Lambda}, \quad (1)$$

where t is the exposure time, N is the number of atoms of ^{10}Be, P_0 is the nuclide production rate at the surface, C_s is the shielding correction, z is the depth below the surface, λ is the decay constant of the radionuclide, and ε is the erosion rate, Λ is the attenuation length, and ρ is the material density. The minimum age is given by assuming negligible erosion ($\varepsilon = 0$), and for samples at the surface (z = 0), equation (1) reduces to

$$t_{\min} = \frac{-1}{\lambda} \ln\left(1 - \frac{N\lambda}{C_s P_0}\right). \quad (2)$$

We use the ^{10}Be production rate and scaling factors of *Stone* [2000]. Uncertainties on the nuclide concentrations include those from the procedural blank, carrier composition, and counting statistics. Errors on the model ages are calculated by propagating the analytical uncertainties together with a 6% error on the absolute production rate [*Stone*, 2000] and a 3.3% uncertainty for the decay constant of ^{10}Be [*Gosse and Phillips*, 2001]. We do not include the variations of the geomagnetic field intensity over time because our sampling sites are located at high latitudes (>62°N) where the variation of the cosmic ray flux is ~1% using the paleointensity data from *McElhinny and Senanayake* [1982] and the Holocene magnetic pole positions from *Ohno and Hamano* [1992] and therefore negligible. All of the isotopic ^{10}Be measurements were made at the Center for Accelerator Mass Spectrometry at Lawrence Livermore National Laboratory. The chemical preparation for ^{10}Be follows *Kohl and Nishiizumi* [1992]. The ^{10}Be CRN model age determinations at Bull Creek and Slate Creek are presented in Table 1. Additional data about the locations and thickness of each sample at both sites appears in the auxiliary material.

3.2. Snow Correction

[19] One of the main concerns regarding the exposure history of a moraine to cosmic rays is the shielding induced by snow cover. This issue cannot be ignored for sites along the snowy southern flank of the Alaskan Range. Snow is a temporary layer that affects the production rate by attenuating

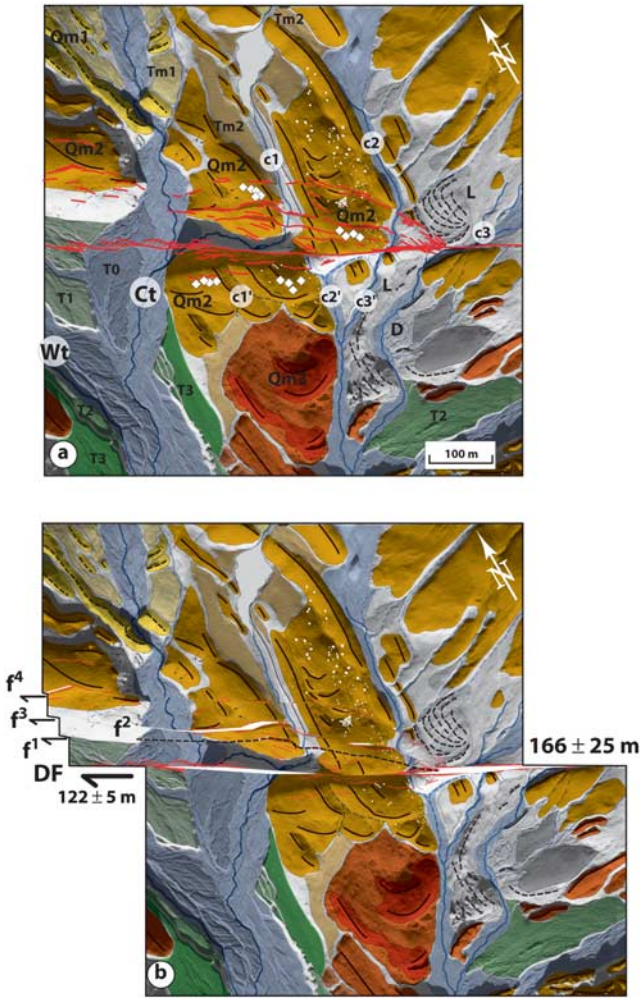

Figure 7. (a) Geomorphic interpretation of the Slate Creek site using the 2002 postearthquake aerial photo with CRN sample locations in white diamonds. Wt and Ct are western and central tributaries, respectively. C1 and C2 are channel 1 and 2 upstream from fault, with their counterpart downstream C1′ and C2′, respectively. Relative age of Quaternary moraines (Qm) and Quaternary terraces (T) are identical than for Figure 6. L indicates landslide and D indicates debris flow. Note line of boulders, sketched in white, on Qm2 bench west of the moraine ridge immediately west of C2, both upstream and downstream from the main fault. (b) Retrodeformation of the Qm2 offset. Secondary faults offsets: f1 + f2 = 9 m, f3 = 19 m and f4 = 16 m. f2 is outline in dash line because it merges with f1 before reaching the west border. The offset on the main strand of Denali Fault is 122 ± 5 m. Note fit of Qm2 moraine crests, boulder lines, and channels (c1, c2, and c3) after retrodeformation of 166 ± 25 m.

a fraction of the cosmic ray flux [e.g., *Gosse and Phillips*, 2001]. To quantify the effect of snow cover, the attenuation of the cosmic rays through a layer of snow is modeled by

$$C_s = \frac{1}{12}\sum_{i}^{12} e^{-[(d_{sm}-d_i)\rho_{sm}/\Lambda]}, \quad (3)$$

where d_{sm} is the monthly average snow cover, d_i is the sample height, ρ_{sm} is the monthly average snow density, and Λ is the attenuation length of cosmic rays through matter. Given the lack of specific information on the snow cover at both sites, the snow corrections were estimated using an average annual snow cover and an average snow density. Assuming an average density for the snow is only a first-order approximation, as snow density may vary greatly, especially with the effect of compaction of high snowpacks. As a result the snow correction applied here cannot be used for large snow depths. We used an average density value with large uncertainties to take into account the large range of possible snow density [*Gosse and Phillips*, 2001]. In addition, as we sampled flat and horizontal ground level cobbles, the height of the sample was neglected in equation (3). Equation (3) thus simplifies to

$$C_s = e^{-(\rho_s d_s/\Lambda)}, \quad (4)$$

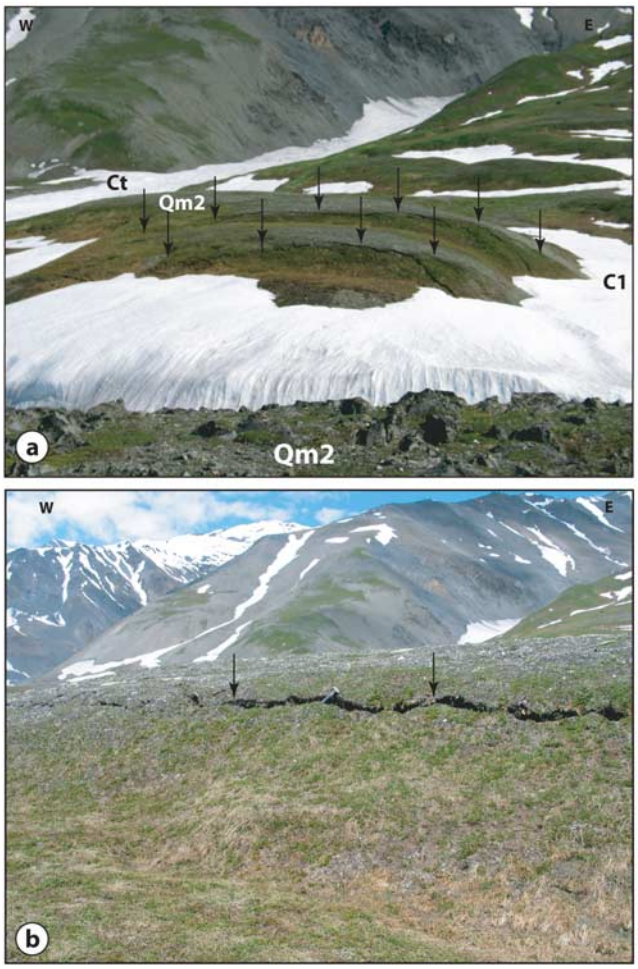

Figure 8. (a) Northward view of the secondary faulting at Slate Creek. Qm2 cumulative offset by f2 and f3 is clearly visible. Normal component represents about 1/4 of horizontal slip on these faults. Arrows point at top of scarps. (b) Closeup of f3. See the Rupture of the 2002 event and cumulative offset along the fault scarp (see hammer for scale). Note that although the apparent slip appear mostly vertical from the photograph, most of the cumulative slip is effectively strike slip.

Table 1. The ^{10}Be CRN Model Age Determinations at Bull Creek and Slate Creek

Sample	NBe[a] (atoms/g of SiO_2 year)	Latitude/Altitude Correction[b] (atoms/g of SiO_2 year)	Shielding Correction[c]	Minimum Be Ages[d] (years)	Snow-Corrected Be Ages[e] (years)
		Bull Creek			
AK03-1	0.132 ± 0.004	2.70	0.94	10244 ± 690	11471 ± 1886
AK03-2	0.157 ± 0.006	2.70	0.94	12296 ± 877	13769 ± 2287
AK03-3	0.148 ± 0.011	2.69	0.98	11140 ± 1067	12475 ± 2220
AK03-4	0.148 ± 0.004	2.69	0.98	11140 ± 735	12475 ± 2044
AK03-5	0.156 ± 0.007	2.70	0.96	11908 ± 895	13335 ± 2237
AK03-6	0.137 ± 0.007	2.69	0.97	10431 ± 824	11681 ± 1980
AK03-7	0.133 ± 0.004	2.69	0.94	10456 ± 703	11709 ± 1925
AK03-8	0.144 ± 0.004	2.69	0.94	11215 ± 743	12559 ± 2060
AK03-9	0.144 ± 0.004	2.69	0.94	11234 ± 745	12580 ± 2063
AK03-10	0.131 ± 0.007	2.69	0.98	9891 ± 797	11076 ± 1886
Mean[f]				10996 ± 750	12313 ± 840
		Slate Creek			
AK03-32	0.183 ± 0.005	3.30	0.97	11262 ± 744	12308 ± 2018
AK03-34	0.201 ± 0.005	3.29	0.98	12311 ± 802	13455 ± 2200
AK03-36	0.178 ± 0.004	3.30	0.94	11249 ± 723	12295 ± 2006
AK03-37	0.166 ± 0.004	3.26	0.95	10534 ± 683	11512 ± 1881
AK03-39	0.156 ± 0.004	3.27	0.95	9866 ± 645	10782 ± 1764
AK03-41	0.186 ± 0.005	3.27	0.95	11768 ± 776	12861 ± 2107
AK03-42	0.168 ± 0.004	3.27	0.95	10600 ± 686	11585 ± 1893
AK03-44	0.125 ± 0.003	3.27	0.95	7882 ± 510	8614 ± 1407
AK03-45	0.190 ± 0.006	3.27	0.93	12280 ± 835	13420 ± 2210
AK03-46	0.185 ± 0.005	3.30	0.94	11776 ± 777	12870 ± 2109
AK03-47	0.149 ± 0.004	3.30	0.95	9315 ± 614	10181 ± 1668
AK03-48	0.167 ± 0.005	3.31	0.96	10351 ± 696	11312 ± 1859
AK03-49	0.165 ± 0.006	3.31	0.95	10301 ± 724	11258 ± 1865
Mean[f]				10730 ± 1254	11727 ± 1370

[a]Propagated analytical uncertainties include error blank, carrier and counting statistics. Concentrations are corrected for the revised half-life of *Nishiizumi et al.* [2007].

[b]Correction factor scaling the sea level high-latitude production rate to altitude and latitude of study sites (SLHL ^{10}Be production rate = 5.1 ± 0.3 atoms/g year [*Stone*, 2000]).

[c]Thickness and topographic or shielding correction beneath flat surface has been calculated considering attenuation of flux coming from all directions, where the flux intensity at depth is $I(x) = I(0)\exp(-\mu L(x))$, attenuation is $\mu = \rho/\Lambda$, and distance through matter is $L(x) = x/\sin(\theta)$, θ being inclination of incoming radiation. A density $\rho = 2.3$ g/cm^3 and attenuation length $\Lambda = 175$ g/cm^2 have been used.

[d]"Zero erosion and no-snow" or minimum model ages are calculated with propagated analytical uncertainties including 6% uncertainty on production rate [*Stone*, 2000], and 3.3 and 2.8% uncertainties for decay constants of 10Be and 26Al respectively [*Gosse and Phillips*, 2001], as well as uncertainty of 10% on density and attenuation length for depth samples.

[e]"Snow-corrected" model ages are calculated as the minimum Be age together with 15% error on the snow correction propagated in quadrature. The snow correction varies from site to site and is detailed in the text.

[f]Error on the mean is ±1 sigma.

where ρ_s (0.25 ± 0.05 g/cm^3) is the average density of snow, d_s is the depth of the annual mean snow cover, and Λ is the attenuation length of cosmic rays through matter (175 ± 17.5 g/cm^2). The historical snow cover can be estimated from meteorological records from the Alaska Snow, Water and Climate Services (http://www.AMBCS.org), averaged over 30 years, and acquired from nearby localities (Figure 9).

[20] The spatial variation of the historical snowpack for the 40 snow stations is available in the area (Figure 9). The snow stations are distributed irregularly and most are close to roads. Despite these limitations, two general trends are clear. Snow accumulation decreases from south to north and from west to east. Overall, the northeastern decrease of snow depth in central Alaska is consistent with the increasing distance between the meteorological stations and the Pacific Ocean, which is the principal source of moisture. Thus, a snow cover correction at Slate Creek, in the east, is likely to be less than for Bull Creek, in the west.

[21] A correction for altitude must also be made [*Schildgen et al.*, 2005]. Both Slate Creek (at 1320 m) and Bull Creek (at 1075 m) are at higher elevations than the measuring stations (43 to 945 m) (Figure 9b). We approximate the average annual snowpack at both sites by extrapolating an exponential function to the snow depth-altitude data of locally selected stations (Figure 9a). The annual mean snow depths at Slate Creek and Bull Creek are estimated to be 66.6 cm and 84.6 cm, respectively (Figure 9a). The altitude correction appears to be rather significant and implies that the snow stations are unlikely to give reasonable estimates of the snow cover at both sites without including further considerations.

[22] Furthermore, the historical data are not likely to reflect the full range of snow conditions during the exposure history of the samples, we must calculate the long-term average by including the relative changes in effective wetness over the last 11 ka, as described by *Benson et al.* [2004]. For this, we use historic lake level records at Birch Lake, which is located north of the Alaska range at about 60 km south of Fairbanks (Figure 1) [*Abbott et al.*, 2000] and the δ^{18}O effective moisture proxy from Meli Lake, located further north in the brooks range at ~67°N [*Anderson et al.*, 2001]. The paleoclimatic records should span the entire exposure history of the samples (~11 ka). But at Birch Lake, the lake level record spans a period from 11 to 5.8 ka, the time at which the lake

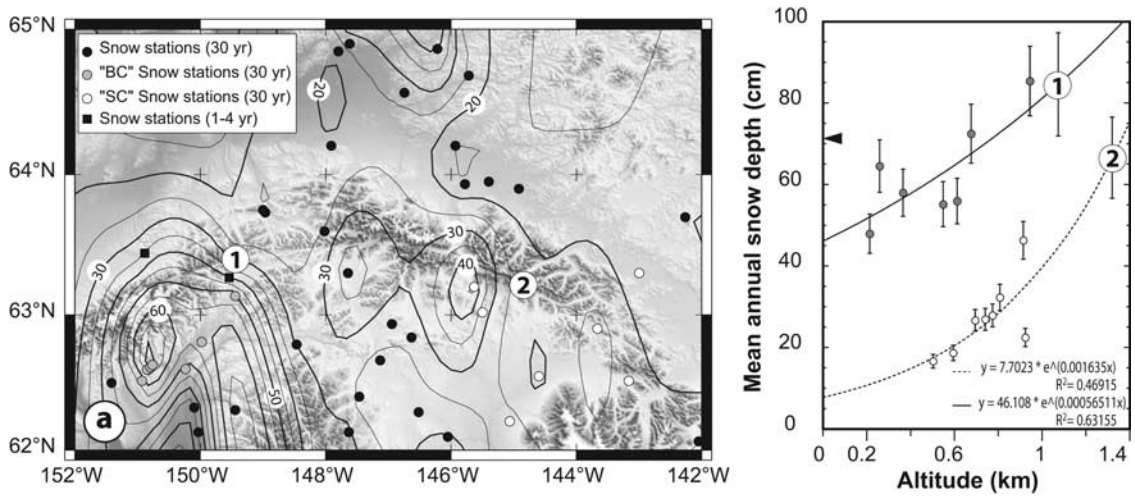

Figure 9. (a) Historical mean annual snowpack (in units of centimeters) along the Alaska Range (www.AMBCS.org) overlaying GTOPO30-DEM map. Sites locations are indicated: 1, Bull Creek; 2, Slate Creek. Meteorological stations are indicated with circles. Stations used to make altitude correction are indicated in gray circles for Bull Creek (BC) and white circles for Slate Creek (SC). (b) Snow dependence with altitude at sites from this study derived from local snow stations and exponential fit. Black arrow indicates the value used by *Matmon et al.* [2006].

started to overflow. At that time, wetter conditions are also observed at Meli Lake [*Anderson et al.*, 2001]. The relative variation of the effective wetness is quite similar for both lakes during the period for which the records overlap (~8.5 to 5.5 ka). Thus, we assume that the relative effective wetness can be used as a regional proxy, and we use the $\delta^{18}O$ records of Meli Lake after 5.8 ka to extend the relative variation of the effective wetness to the present conditions. In summary, the relative variation of moisture proxies shows that the wet and cool Younger Dryas (YD) event at ~11.5 ka evolved over 5 ka from drier to wetter conditions. After ~6 ka, the relative effective moisture proxy is relatively constant and oscillates around the present conditions. Overall, taking the combined relative changes in effective wetness, the historical snowpack data are relatively wetter by 6% than long-term conditions. Therefore, historical values overestimate by 6% the 11-ka average. Consequently, the trans-Holocene annual snow cover estimates for Slate Creek and Bull Creek are 62.6 cm and 79.5 cm, respectively. Ultimately, the snow corrections calculated from equation (4) increase the CRN surface exposure ages by 8.5% and 10.7% at Slate Creek and Bull Creek, respectively.

[23] Note that the long-term correction only applies to samples exposed to cosmic rays for the last 11 ka. Younger and older samples have likely experienced different snow conditions. This is clearly the case for older samples that would have been exposed to the severe snow conditions of the Younger Dryas glaciation and that might have been totally shielded during that time [*Schildgen et al.*, 2005]. This implies that comparison of model ages of different exposures can be seriously biased without considering the variation of snow condition through time. Finally, the corrections applied at both sites do not take into account other local snow conditions such as the effect of wind and the local topography but rather try to quantify the common shielding of snow at a given altitude and over a given exposure to correct the CRN model ages and allow to compare results from different locations. Considering the complexity of that correction, it appears difficult to quantify its uncertainty but it cannot be ignored. Here, the error on these snow corrections is taken to be 15%, which could be underestimated if the local snow conditions are significant. If the altitude and the long-term corrections were not estimated to calculate the snow shielding and correct the ^{10}Be model ages, the error of that correction would be closer to 50%.

[24] Aside from the effect of the snow cover, secondary effects such as erosion, surface deflation and exhumation could also affect the CRN model ages toward younger apparent values. However, these effects are unlikely to affect all the samples similarly. Consequently, a broad CRN model age distribution would be expected if these effects were significant and vice versa. We will next show that this was not the case in our study.

3.3. The ^{10}Be CRN Model Ages

[25] We determined the timing of moraine emplacement at both sites using ^{10}Be CRN dating of quartz-rich samples. At Bull Creek, we sampled 10 large cobbles (8–26 cm, auxiliary material) embedded in the well-preserved Qm2 moraine immediately west of the offset moraine crest and south of the fault trace. We chose the largest available flat and horizontal samples on the moraine downstream and avoided the degraded upstream side of the moraine. This sampling strategy minimized the possibility of collecting samples deposited by the erosion of the adjacent older moraine and the eastern steep flank of the glacial valley EO. The CRN model ages range from 9.9 ± 0.8 ka to 12.3 ± 0.9 ka and yield an average model age of 11.0 ± 0.8 ka (n = 10, ± 1σ, Figure 10). The age distribution is exceptionally narrow for CRN surface exposure dating and shows a normal distribution with an MSWD of 0.84. This narrow distribution indicates that effects of erosion, surface deflation and exhu-

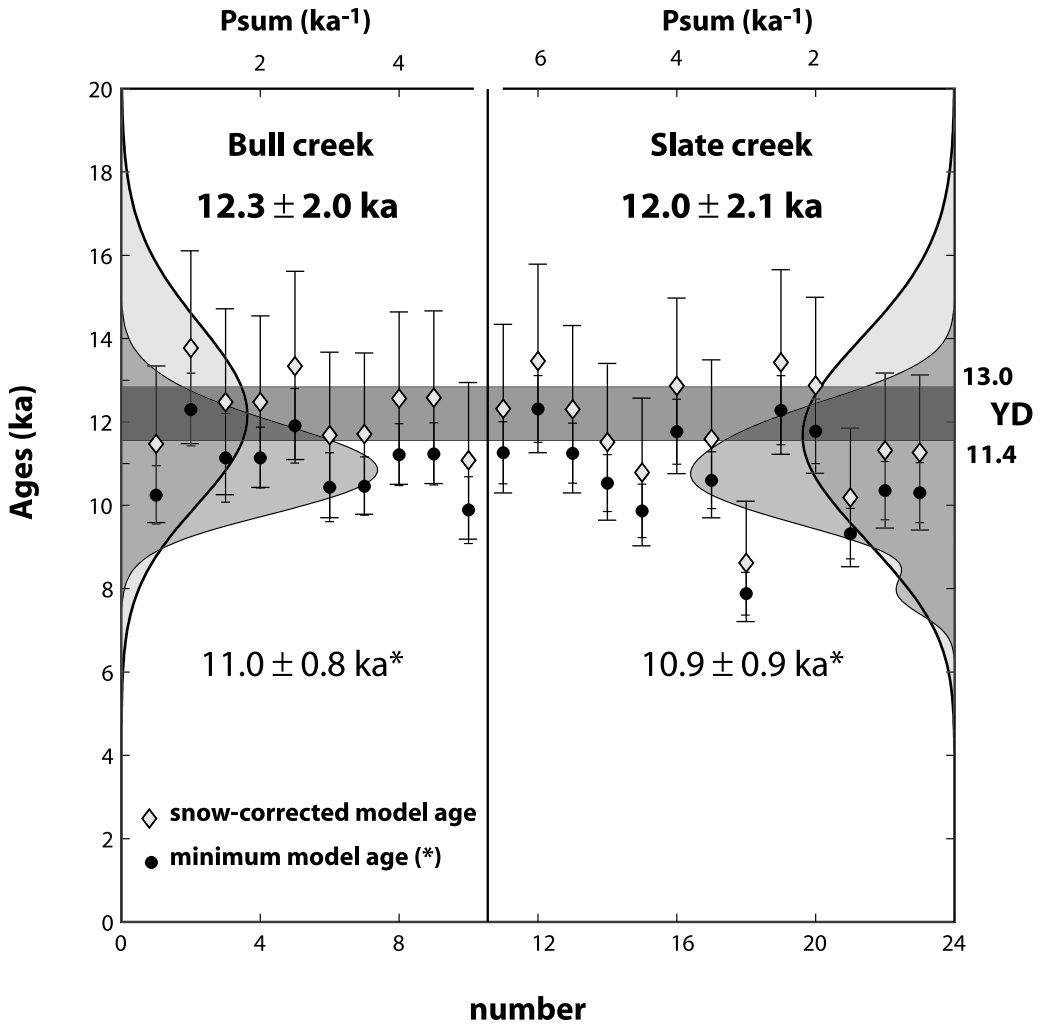

Figure 10. The ^{10}Be CNR model ages at both sites with cumulative distribution of data (Psum as defined by *Daëron et al.* [2004]) with and without the snow correction and comparison with the Younger Dryas [*Alley et al.*, 1993; *Alley*, 2000]. The mean of minimum (indicated by an asterisk) and snow-corrected (indicated by boldface) CRN model ages are indicated.

mation have been limited on that moraine. The snow-corrected model ages are older by 8.5% and yield an average age of 12.3 ± 2.0 ka (±1σ).

[26] At Slate Creek, we sampled 13 large embedded cobbles (8–27 cm, auxiliary material) from a set of Qm2 moraines on both sides of the Denali Fault and on both side of channel c1 (Figure 7). The samples upstream from the main fault trace came from moraines also cut and offset by secondary splay faults (Figures 7 and 8). Similar to our sampling at Bull Creek, we sampled the largest available flat and horizontal cobbles, leaving boulders and pebbles aside. The model ages range between 7.8 ± 0.5 ka and 12.3 ± 0.8 ka, and the average age is 10.7 ± 1.3 ka (n = 13, ± 1σ, Figure 10). This determination is indistinguishable from the mean CRN surface exposure ages obtained at Bull Creek. As at Bull Creek, the age distribution at Slate Creek is narrow, although the youngest sample (AK03-44, 7.8 ± 0.5 ka) is defined as an outlier using Chauvenet's criterion [see *Bevington and Robinson*, 2002, p. 58]. The remaining age distribution is normally distributed with an average of 10.9 ± 0.9 ka (n = 12, ± 1σ) with an MSWD of 1.78. The snow-corrected model ages are older by 12.5%, with an average of 11.7 ± 2.2 ka (±1σ). If we exclude the defined outlier, we obtain an average snow-corrected age of 12.0 ± 2.1 ka. Thus, it appears that the dated moraines from both sites are synchronous and show a normal distribution of ages, with a mean snow corrected age of 12.1 ± 1.0 ka (n = 22, 1 outlier, ± 1σ) and an MSWD of 0.23.

[27] The moraine sampling strategy of this study differs from most common sampling for CRN dating as no boulders were sampled [i.e., *Gosse and Phillips*, 2001; *Briner et al.*, 2005]. Boulders at the sites of study were either lacking, had complex geometries, clear evidences of erosion, and/or fractures compared to the embedded flat and horizontal cobbles that were sampled (auxiliary material). Cobbles and boulders are affected differently by external factors. Small samples of cobbles or pebbles are considered to be more easily exhumed and reworked compared to boulders [i.e., *Farber et al.*, 2005]. The entire snow cover shields cobbles while boulders have a lesser snow cover as they stand above ground. Small samples embedded at the ground level are not affected by wind erosion while boulders are [i.e., *Kaplan et al.*, 2005;

Table 2. Slip Rate Estimates at Bull Creek and at Slate Creek[a]

	Bull Creek	Rate (mm/a)	Slate Creek	Rate Using USGS's Estimate[b] (mm/a)	Rate Using This Study (mm/a)	Rate Using Taylor's Estimate[c] (mm/a)
Cumulative Offset (m)	82 ± 5			122 ± 5[d]	166 ± 25	183 ± 30[e]
Coseismic 2002 slip (m)				5.0 ± 0.3[d]	6.8 ± 1.0	7.5 ± 1.1[e]
"Minimum Be" mean age (ka)	11.0 ± 0.8	7.5 ± 0.7[e]	10.7 ± 1.3	10.9 ± 1.5[d]	14.9 ± 3.6[e]	16.4 ± 4.1[e]
"Snow-corrected" mean age (ka)	12.3 ± 2.0	**6.7 ± 1.2**	11.7 ± 1.4	10.0 ± 2.0[d]	13.6 ± 3.8	15.0 ± 4.4[e]
			12.0 ± 2.1[f]	9.8 ± 1.1[d]	**13.3 ± 3.6**	14.6 ± 4.1[e]
Younger Dryas (ka)	12.3 ± 0.8	**6.7 ± 0.6**	12.3 ± 0.8	9.6 ± 0.9[d]	**13.0 ± 2.9**	14.4 ± 3.3[e]

[a]Error is ± 1σ for the surface exposure mean age. "Snow-corrected" means include the 15% error of the snow correction propagated in quadrature. The age of the Younger Dryas is the estimate of *Alley et al.* [1993] and *Alley* [2000]. Errors on the slip-rates are obtained by propagating the error on the offset and age in quadrature. Bold values are the most likely slip-rate estimates at each site (See text for details).
[b]*Haeussler et al.* [2004].
[c]*Taylor et al.* [2008].
[d]Minimum slip rate estimates using minimum offset estimate (see text for detail).
[e]Maximum slip rate estimates using the uncorrected minimum Be mean age (see Table 1) and/or maximum offset estimates.
[f]"Snow-corrected" mean at Slate Creek without the defined outliner (AK03-44).

Briner et al., 2005]. Thus, the corrections to apply for CRN model ages between boulders and cobbles are expected to be different. The effect of size on CRN model ages remains mostly unconstrained. In this study, we have a posteriori tested the effect of sample size to CRN model ages. We measured the long and small axis of each sample from field photographs to estimate the surface area exposed to cosmic rays and plotted these as a function of the CRN model ages (auxiliary material). In the size range that we sampled, there is no clear correlation between the size and the CRN apparent ages. The largest samples at Slate Creek appear biased toward younger values whereas the tendency seems slightly reversed at Bull Creek (auxiliary material). A further examination of the field pictures at Slate Creek revealed that these apparent younger big samples had either a more complex pyramidal geometry (AK03-44) or were fractured (AK03-47) (see the auxiliary material). These observations alone could explain the apparent young CRN model ages. Overall, cobbles that were flat and horizontal seem to describe a Gaussian distribution of the CRN model ages, which to some extent validates the sampling strategy used at both sites.

[28] The dated moraines (12.1 ± 1.0 ka, ± 1σ) at both studied sites appear to be roughly coeval with the Younger Dryas cooling chronozone (12.8 ± 0.2 ka to 11.6 ± 0.1 ka [*Alley et al.*, 1993] and revision for the end of the event at 11.5 ± 0.2 ka by *Alley* [2000] (Figure 10), and are also roughly consistent with a peak in the probability distribution of moraine ages (~10–13 ka) from Alaska summarized by *Briner et al.* [2005]. Indeed, based on moraine CRN ages from the Ahklun Mountains of southwestern Alaska, *Briner et al.* [2002] determined that the Mt. Waskey advance culminated between 12.4 and 11.0 ka, sometime during, or shortly following, the Younger Dryas event (~12.9–11.6 ka), and conclude that the Mount Waskey advance was a consequence of cooling during the Younger Dryas. Although evidence of drastic climatic fluctuations during the Younger Dryas chronozone have been inferred from other studies in North Pacific region including in Alaska [*Engstrom et al.*, 1990; *Gosse et al.*, 1995a, 1995b; *Abbott et al.*, 2000; *Anderson et al.*, 2001; *Briner et al.*, 2002; *Kovanen and Easterbrook*, 2002; *Friele and Clague*, 2002; *Hu and Shemesh*, 2003; *Hu et al.*, 2003; *Lacourse*, 2005; *Cook et al.*, 2005; *Lakeman et al.*, 2008], the global/regional extent of YD cooling remains much debated [cf. *Hu et al.*, 2006; *Carlson*, 2008]. Nevertheless, it is reasonable to surmise from the coincidence in the CRN model ages that the glacial advance represented by the offset moraines occurred during the Younger Dryas chronozone. Given the well-defined duration of the Younger Dryas (11.4 to 13 ka or 12.2 ± 0.8 ka) we choose to use this narrower temporal constraint on the Younger Dryas chronozone below, to reduce the impact of CRN model age assumptions and snow correction uncertainties in the slip rate uncertainties. We use hereafter the age of the YD cooling event (12.2 ± 0.8 ka) together with our snow-corrected CRN dating (Bull Creek: 12.3 ± 2.0 ka; Slate Creek: 12.0 ± 2.1 ka) to estimate the slip rate at each site.

3.4. Slip Rates Along the Denali Fault

[29] Linking the surface exposure ages with the moraine offsets yields millennial slip rates for the Denali Fault at these two localities (Table 2). At both sites, we have good reasons to believe that the retreating glacier left features that were nearly linear where they crossed the fault, as none of the features display any near-fault irregularities in their trend. Thus, the offsets record slip that accrued after the glacier stopped sculpting or moving the moraine.

[30] At Bull Creek, the average snow-corrected surface exposure age of 12.3 ± 2.0 ka and the 82 ± 5 m offsets of the Qm2 lateral moraine and its marginal ice channel yield a Holocene slip rate of 6.7 ± 1.2 mm/a (Table 2 and Figure 11). Using the more narrowly defined age of the Younger Dryas cooling chronozone, 12.2 ± 0.8 ka [*Alley et al.*, 1993; *Alley*, 2000], as the age of this offset yields an identical slip rate but with a smaller error of 6.7 ± 0.6 mm/a. A maximum slip rate estimate of 7.5 ± 0.5 mm/a results from the use of the uncorrected CRN model ages (Table 2).

[31] At Slate Creek, the slip rate estimates are somewhat more complex due to the distribution of the deformation. However, bounds on the slip rate can be easily estimated. To define the average Holocene rate at Slate Creek, the amount of displacement during the 2002 event is to be subtracted from the cumulative offset. The cumulative offset estimates considered in deriving the slip rate are 122 ± 5 m, 166 ± 25, and 183 ± 30 m. The estimated coseismic offsets associated with these cumulative, long-term offsets are 5 ± 0.3 m, 6.8 ± 1.0 m, and 7.5 ± 1.1 m, respectively. In considering the three offset and age determinations, the discussion hereafter is limited to the estimates based only on the Younger Dryas age. The remaining slip rate estimates are nonetheless indicated in Table 2. Again, using the well-defined 12.2 ±

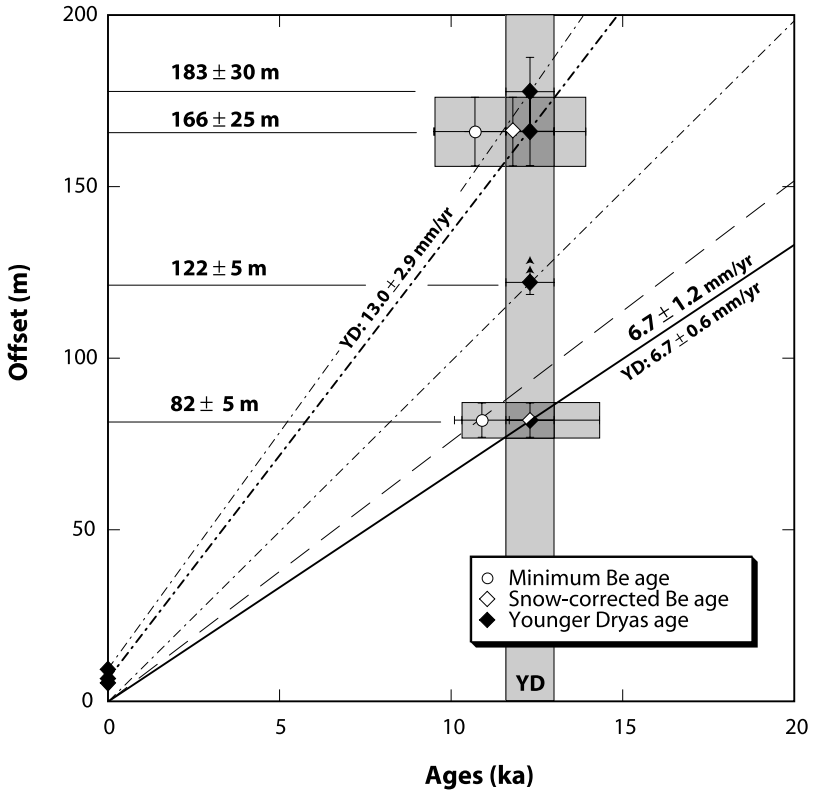

Figure 11. Slip rate diagram using the different ages estimates of the uncorrected and snow-corrected surface exposure ages (Table 2), and of the Younger Dryas (YD) [*Alley et al.*, 1993; *Alley*, 2000]. Arrows for 122 ± 5 m indicate that this offset is a minimum bound. Dash lines represent the various slip rates derived from each dated offsets (see Table 2). Bold dash lines with slip rate values are best estimated (see text for detail).

0.8 ka age of the Younger Dryas [*Alley et al.*, 1993; *Alley*, 2000] together with the offsets defined above, slip rates of 9.6 ± 0.9 mm/a, 13.0 ± 2.9 mm/a, and 14.4 ± 3.3 mm/a are obtained, respectively (Figure 11, Table 2).

[32] Unlike at Bull Creek, the slip rate estimates at Slate Creek are bracketed by uncertainty in the offset determinations rather than the age determinations. As deformation at Slate Creek is not limited to main trace of the fault but rather distributed over numerous fault strands, the estimate of 9.6 ± 0.9 mm/a defined by considering only the cumulative and coseismic offsets on the main trace of the fault is obviously a minimum bound. The third estimate of 14.4 ± 3.3 mm/a is obtained by multiplying the cumulative offset measured on the main strand (122 ± 5 m) by the ratio of the total coseismic slip estimate [*Taylor et al.*, 2008] and the coseismic slip on the main strand of the fault [*Haeussler et al.*, 2004]. This rate is a maximum bound and is the most poorly defined. Indeed, it would imply a constant slip ratio between the main trace and the secondary faults since the emplacement of the Qm2 moraines, which is unlikely considering the rupture complexity. The intermediate slip rate of 13.0 ± 2.9 mm/a appears the most reliable determination at Slate Creek as it takes carefully into account both the estimated coseismic and cumulative displacements that offset Qm2. The rate obtained relies on our ability to measure both coseismic and cumulative offsets within a complex fault zone. As some fraction of the total offset will be "unobserved" in the field, it is likely that the summed offsets used in these determinations underestimate the true cumulative offset. Regardless of nonsystematic uncertainty, the slip rate estimates obtained above are quite comparable (in agreement at the 1-sigma level), indicating that the distribution of the deformation between the main trace and the secondary faults tends to remain relatively constant over the Holocene. Overall, we observe an unambiguous westward decrease of the rate along the Denali from about 13 mm/a to 7 mm/a, as both offset Qm2 moraines have similar exposure age of 12.1 ± 1.0 ka (n = 22 CRN model ages, ± 1σ). Therefore, the derived rates rely solely on the observed westward decrease of the offset measurements at both sites.

[33] The slip rate determinations from this study and those of *Matmon et al.* [2006] are given in Figure 12. The slip rates in this study are comparable to the estimates of *Matmon et al.* [2006] on the Denali Fault despite their somewhat different methodology: rough offset measurements, variable number of samples per offset (two to four for five sites and seven and 11 for the two remaining sites, respectively), different sampling strategy (boulders and sediments) and the application of an unique snow shielding correction for all their CRN model ages at all their sites. At Slate Creek, our slip rate results differ from the rate of *Matmon et al.* [2006], mostly as their offset estimate of Qm2 does not take in account any secondary faulting contribution. However, the mean rate on the Denali Fault of both studies is in broad agreement with 9.9 ± 4.5 mm/a for this study and 10.0 ± 2.7 mm/a for *Matmon et al.* [2006]. In

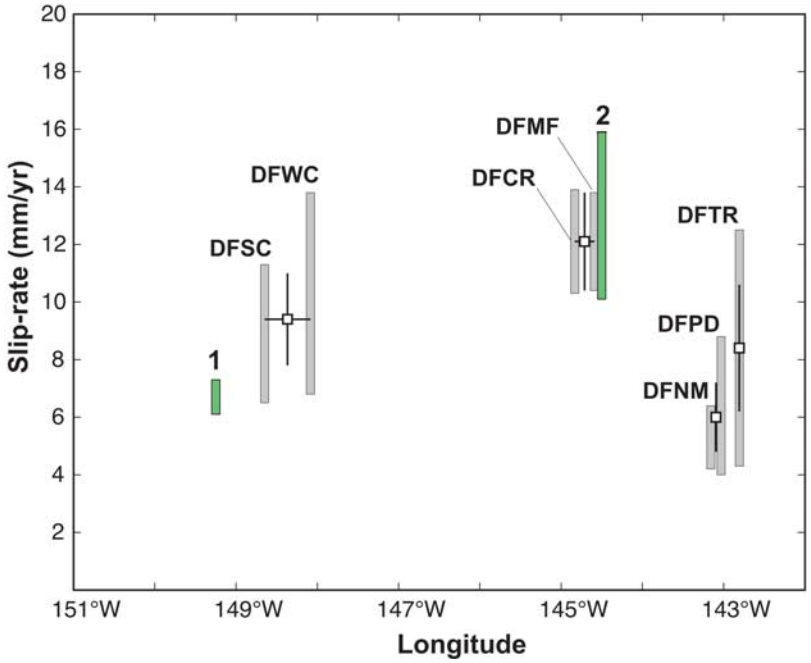

Figure 12. Slip rate variations of this study (green boxes) and of *Matmon et al.* [2006] (gray boxes). Numerals 1 and 2 indicate the rates at Bull Creek and Slate Creek of this study, respectively. Grey boxes indicate the range of rates derived at each site by *Matmon et al.* [2006]. Whites squares indicated the average rates of each fault segment as published by *Matmon et al.* [2006]. Site names of *Matmon et al.* [2006] are also indicated.

this study, the increased uncertainty of the average reflects mostly the significant along-strike westward decrease of the slip rate of the Denali Fault. Most importantly, the rate that we obtain at Bull Creek on the western segment of the Denali Fault is significantly lower than the rate obtained along the central portion of the fault (Figure 12), and verifies the suggested westward decrease of the slip rate on the Denali Fault between the central Denali Fault and the western Denali Fault [*Mériaux et al.*, 2004b; *Matmon et al.*, 2006].

4. Kinematic Behavior of the Alaska Range

[34] The most common model for the Denali Fault is that the right-lateral strike-slip fault accommodates the counterclockwise vertical axis rotation of southern Alaska [*St. Amand*, 1957; *Lahr and Plafker*, 1980; *Stout and Chase*, 1980; *Page et al.*, 1995]. Such a model implies a uniform fault slip rate along the entire length of the Denali Fault and that motion of the Wrangell block is decoupled from the Alaska Range to the north. This model is clearly not supported by our slip rate determinations, which demonstrate the motion along the Denali Fault during the Holocene is characterized by a westward decreasing lateral slip; a decrease of roughly 50% between 149°W and 145°W, which indicate a northwestward translation of southern Alaska and slip partitioning between the arcuate strike-slip Denali Fault and neighboring folds and thrust faults. At the very least, the westward decrease in the fault's slip rate requires a modification of the counterclockwise rotational model for the Denali Fault.

[35] To accommodate the slip rate variation along the Denali Fault, we propose a new tectonic model in which northwestward translation of southern Alaska results in a westward increase in the partitioning of slip from the arcuate strike-slip Denali Fault to neighboring folds and thrust faults to the north. Consistent with the model, the northern flank of the Alaska Range displays a topographic scarp consistent with an active north-directed thrust system [*Bemis*, 2004; *Bemis and Wallace*, 2007; *Lesh and Ridgway*, 2007] (Figures 13 and 14). Furthermore, the Alaska Range widens from east to west, suggesting that crustal thickening becomes the dominant process as Mt. McKinley is approached from the east. Thus, the active structures of the Alaska Range northeast of the Denali are genetically linked to its strike-slip motion and play a critical role in accommodating translation of southern Alaska. We postulate that the geometry, kinematics, and style of deformation for the Denali Fault and the Northern Foothills thrust system can, therefore, be explained by northwest translation of the Wrangell block.

[36] *Bird* [1996] proposed a kinematic model for southern Alaska with features similar to that proposed here. His preferred result indicates a slip rate of 13 mm/a, such as Slate Creek, on the segment of the Denali Fault between Little Tok river and Delta river, which decreases to 6 mm/a near longitude 150°W. However, crustal thickening near and to the west of 150°W, is accommodated to the south of the Denali Fault on the southeast-directed Broxson Gulch and Pass Creek thrust faults [*Stout and Chase*, 1980; *Plafker and Berg*, 1994] unlike our model that proposes a preferential transfer of the deformation to the north.

[37] A vector diagram of our kinematic model of southern Alaska that incorporates northwest translation of southern Alaska relative to stable North America along azimuth N226° is shown in Figure 13. This azimuth results from a

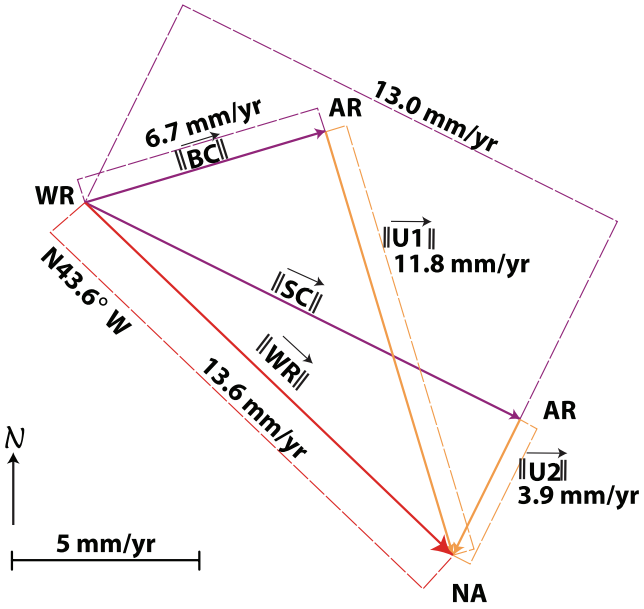

Figure 13. Vector diagram illustrates the kinematics of Alaska Range using the slip rate estimates at Bull Creek (BC) and Slate Creek (SC), assuming no rotation (see text for detail). N44°W translation of the Wrangell block (WR) is estimated to be ~14 mm/a. AR, Alaska Range; U1, Bull Creek convergence rate; U2, Slate Creek convergence rate.

vector diagram that incorporates the slip rate estimates determined for the Bull and Slate Creek sites. A point in the diagram represents each block of the system, and the connecting lines represent the faults that bound them. The blocks include Wrangellia (WR), the Alaska Range (AR), and stable North America (NA). The vectors BC and SC are the Bull and Slate Creek segments of the Denali Fault, respectively, and represent the fault strike and slip rate magnitude.

[38] The translation direction of the WR block is determined by assuming that the east to west decrease in fault slip rate results from the transfer of dextral strike slip on the Denali Fault in the east to reverse faults of the Alaska range in the west. To simplify the calculation, we assume a convergence component perpendicular to the strike of the Denali Fault strike at any point and no block rotation. The intersection of the convergence components for two sites represents the azimuth and velocity of the WR block with respect to NA. This kinematic model predicts increasing convergence rates between Slate Creek, ~4 mm/a, and Bull Creek, ~12 mm/a. This observation is consistent with the geometry of the Alaska Range, which is ~30 km wide near Slate Creek and ~50 km near Bull Creek. This implies that the width of the Alaska Range is dependent upon the strike of the Denali Fault and the northwestward translation of Wrangellia and that this kinematic relationship is a long-term feature that has persisted over the growth history of the Alaska Range. The model also predicts that the rate of translation of WR block is 13.6 mm/a. However, as no block rotations were assumed here, only maximum uplift estimates are derived. Indeed, any small rotation of southern Alaska would result in a decrease in the uplift rate along the Alaska Range and more specifically to the west.

[39] The proposed westward increase in the slip partitioning from the Denali Fault to the Alaska Range requires the existence of active structures that accommodate the deformation within the Alaska Range. Although there are some candidate structures located both north and south of the Denali Fault, the segmentation of the fault system and the main triple junctions are difficult to pinpoint in such glaciated environments, unless recently activated. For instance, active

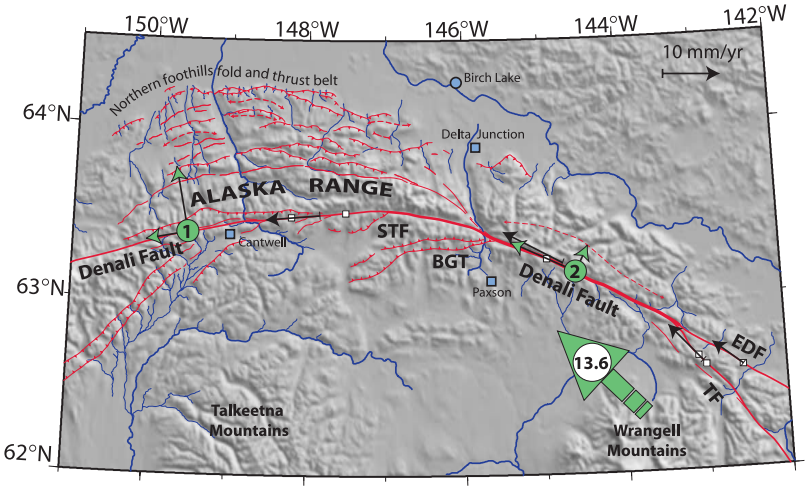

Figure 14. Tectonic map of the Denali Fault system along the Alaska Range between 142°W and 151°W. Fault mapping is modified from *Plafker and Berg* [1994, and references therein]. Mapping of northern Alaska Range is more specifically derived from *Bemis* [2004]. EDF, Eastern Denali Fault; STF, Sustina Glacier Fault; BGT, Broxson Gulch Thrust. Site locations and rates of this study are green circles and green arrows, respectively (1, Bull Creek; 2, Slate Creek). Note that both strike-slip and convergence rates are indicated. Site locations and average rates of *Matmon et al.* [2006] are indicated white squares and black arrows, respectively. Note the convergence rate of WR (~14 mm/a) inside green arrow derived from this study.

structures would include the Susitna Glacier thrust that ruptured in 2002 [*Crone et al.*, 2004] or the southeast directed thrust faults located at the apex of the Denali Fault (Figure 14) [*Stout and Chase*, 1980; *Bird*, 1996]. The north flank of the Alaska Range is another potentially active fault system as pointed out by recent studies [*Bemis*, 2004; *Bemis and Wallace*, 2007]. Such activity is consistent with the deformed Pleistocene Nenana deformed gravels, which are cut by thrust faults and warped into north-verging folds [*Bemis*, 2004; *Bemis and Wallace*, 2007]. Further neotectonic studies are needed to quantify the rate of deformations within this fold and thrust belts and in particular on the northern frontal thrust (Figure 14). If most of the transfer of slip is into the northern Alaska Range, then the maximum convergence rates at 149°W and 145°W should be about 12 mm/a and 4 mm/a, respectively. These uplift rates represent clearly maximum bounds for the active structures north of the Denali Fault, as a portion of the deformation is also accommodated, to a lesser degree, by the active structures south of the Denali Fault, as shown with the rupture of the Susitna Glacier Fault in 2002.

5. Conclusions

[40] Using CRN dating to constrain the age of moraine offsets at two sites on the Denali Fault, we demonstrated the westward decrease in the Holocene slip rate suggested by *Matmon et al.* [2006]. In our study, the mean concentration of ^{10}Be on the moraines at both sites is indistinguishable. So, while snow cover and production rate models may influence the absolute ages and derived slip rates, our estimate of the westward decrease in slip rate is robust. Perhaps the most striking feature of the spatial distribution of slip rate is that it is also reflected at both decadal and geologic timescales by both the recently observed distribution of coseismic slip [*Eberhart-Phillips et al.*, 2003; *Hreinsdottir et al.*, 2003; *Wright et al.*, 2004; *Haeussler et al.*, 2004] and topography, respectively. This suggests that the kinematics recorded in the long-lived geologic structures and topography in this region is equivalent to the one that characterize the earthquake cycle. Thus, the 2002 Mw7.9 Denali earthquake is likely a characteristic earthquake for the Denali Fault. Given the rate of 13.0 ± 2.9 mm/a derived at Slate Creek, along with the coseismic displacement of 6.8 ± 1.0 m, the recurrence time of such a characteristic earthquake would be 525 ± 137 years. Hence, a penultimate event, such as the 2002 quake, would have occurred sometime between 1560 and 1285 years B.P., in keeping with the preliminary results of *Schwartz* [2003].

[41] The correlated asymmetry among coseismic offset, slip rate, and width of associated shortening along the Denali Fault is consistent with a constant recurrence interval for a characteristic earthquake. This is in contrast to other faults, such as the Kunlun Fault, a sinistral strike-slip fault of similar length in central Tibet. Unlike the Denali Fault, the Kunlun Fault is not associated with large-scale, active shortening features, and the slip rate on the Kunlun Fault is remarkably constant along strike [*Van der Woerd et al.*, 2002]. However, the inferred characteristic coseismic offset is larger along the western segments of the fault than along it eastern segments, requiring that the constant slip rate is modulated by variable recurrence interval, while the variation of the slip rate on the Denali Fault appears modulated by variable coseismic offset. This comparison suggests that offset magnitude recurrence behavior of a fault is influenced not only by local fault zone mechanics, but also by the large-scale structure, segmentation, and slip distribution among associated faults.

[42] The westward decrease in the long-term slip rate on the Denali Fault has critical implications for the growth of the Alaska Range. In contrast to previous models which invoke rotation of southern Alaska as the primary active tectonic mechanism, we conclude that the Wrangell block is translating to the northwest at a rate of about 14 mm/a and that a portion of that deformation is progressively transferred to the northern Alaskan range reaching convergence rates of ~12 mm/a to the west. Deformation from the Aleutian megathrust is transferred inland, first by strike-slip faulting, and then even further north by transfer of deformation to shortening features resulting in topographic uplift. As such, slip partitioning is a critical mechanism in understanding intracontinental deformation in southern Alaska.

[43] The association of dip-slip structures with long-lived strike-slip faults is rather common [e.g., *Henyey and Wasserburg*, 1971; *Gaudemer et al.*, 1995; *Armijo et al.*, 1996; *Meyer et al.*, 1998]. The association of faults with contrasting kinematics, slip partitioning, was proposed to be an effect of oblique slip at depth that is accommodated by several fault systems at the surface [e.g., *Armijo et al.*, 1986; *Bowman et al.*, 2003]. Implications for the seismic behavior in such partitioned systems are critical in forecasting subsequent seismicity. If the strike slip-oriented component of stress in such system is released by a large strike-slip event, such as the November 2002 Denali Fault earthquake, then the postearthquake stress field is more likely to exhibit enhanced dip-slip-oriented stress [*Bowman et al.*, 2003]. However, the dip-slip component is often short-lived and the seismic behavior of such transitory system is poorly understood. Given the observed Denali-Alaska Range slip partitioning, the strike-slip nature of the Denali earthquake may favor future dip-slip seismicity in the Alaska Range. The role of the suggested enhancement of dip-slip stress in the Alaska Range must be balanced against enhanced stress at the tips of the strike-slip rupture [*Stein et al.*, 1992; *King et al.*, 1994], which has been shown to play a predominate role in stress propagation along other large strike-slip faults such as the North Anatolian Fault [*Hubert-Ferrari et al.*, 2000]. However, not only was the Denali earthquake a slip-partitioned event [*Eberhart-Phillips et al.*, 2003], but the stress regime following this event alternated between strike slip and thrusting along the rupture [*Ratchkovski et al.*, 2004], indicating that the accumulated composite stress do not necessarily release alternatively. In fact, slip partitioning seems to coexist simultaneously at all timescales, from the seismic cycle to the mountain building timescale. However, the succession of events of different pure mechanisms is also present in the area. The large thrusting event in the Alaska Range, the M ~ 7.2 1947 event followed the M ~ 7.2 1912 Delta River earthquake on the Denali Fault [*Page et al.*, 1991; *Carver et al.*, 2004]. From that point of view, the seismic behavior of such partitioned system appears to reflect the instability of such system at all timescales. Thus, the release of the partitioned stress in a single complex event rather than in a strike slip and thrust events should mostly be an effect of the geometry and segmentation of the partitioned fault system.

[44] At longer timescales, slip partitioning is a key in the understanding of the evolution of large continental fault systems. In fact, slip partitioning has often been interpreted as a part of the propagation of the long-lived strike-slip fault systems such as the Altyn Tagh and Haiyuan Faults in northern Tibet [e.g., *Peltzer and Tapponnier*, 1988; *Gaudemer et al.*, 1995] or the North Anatolian Fault in Anatolia [e.g., *Armijo et al.*, 1999]. Fault propagation is often associated with increased fault segmentation together with slip rates on the main strand of the fault that decrease along strike in the direction of propagation. In Tibet, in particular, along-strike decreases in slip rate have been documented for both the Altyn Tagh Fault [*Mériaux et al.*, 2004a, 2005] and the Haiyuan Fault [*Lasserre et al.*, 1999, 2002]. In a similar connection, the lateral slip rate on the North Anatolian Fault decreases as lateral motion is transferred to extension on the subperpendicular Corinth Fault system [*Armijo et al.*, 1996]. The Denali Fault seems to follow the same rules with a significant decrease of slip rate together with the widening of the Alaska Range as a result of the increase in the convergence rate to the west.

[45] At a continental scale, some of the largest strike-slip faults have been associated with the large-scale intracontinental extrusion of semirigid continental blocks extruding at high angle to the direction of convergence, e.g., eastward extrusion of Indo-China along the Red River Shear Zone [*Leloup et al.*, 1993] and westward extrusion of Anatolia along the North Anatolian Fault [*Armijo et al.*, 1999]. At a smaller regional scale, the Denali Fault seems to facilitate the extrusion of southern Alaska as a result of the oblique convergence of the Yakutat block. However, the largest share of this deformation has not yet been transferred inland to the strike-slip fault systems of southern Alaska, but it is still localized south of the Border Ranges Fault and within the syntaxis that accommodate on the order of 30 mm/a of convergence rate, given the ~14 mm/a left on the Wrangell block.

[46] **Acknowledgments.** The sample processing and dating work was performed under the auspices of the U.S. Department of Energy, at the University of California Lawrence Livermore National Laboratory, under contract W-7405-Eng-48 and under the sponsorship of the Laboratory Directed Research and Development program (UCRL-JRNL-228719). Field work was supported by the Gordon and Betty Moore Foundation, through the Tectonics Observatory at Caltech, and by grant NAG5–10406 from NASA to KS. This work was also supported by NSF research grant EAR-0107114 to CMR. We are grateful to John Galetzka, Ana Cadena, and Keegan Fengler for their help with the total station measurements. We thank J. Gosse and an anonymous reviewer for their thoughtful reviews together with the associate editor Gideon Rosenbaum for his comments. This is University of California UCRL- JRNL-228719 and Tectonics Observatory contribution 98.

References

Abbott, M. B., B. P. Finney, M. E. Edwards, and K. R. Kelts (2000), Lake-level reconstructions and paleohydrology of Birch lake, central Alaska, based on seismic reflection profiles and core transects, *Quat. Res.*, *53*, 154–166, doi:10.1006/qres.1999.2112.

Alley, R. B. (2000), The Younger Dryas cold interval as viewed from central Greenland, *Quat. Sci. Rev.*, *19*, 213–226, doi:10.1016/S0277-3791(99)00062-1.

Alley, R. B., et al. (1993), Abrupt increase in Greenland snow accumulation at the end of the Younger Dryas event, *Nature*, *362*, 527–529, doi:10.1038/362527a0.

Anderson, L., M. B. Abbott, and B. P. Finney (2001), Holocene climate inferred from oxygen isotope ratios in lake sediments, Central Brooks Range, Alaska, *Quat. Res.*, *55*, 313–321, doi:10.1006/qres.2001.2219.

Armijo, R., P. Tapponnier, J. L. Mercier, and T. L. Han (1986), Quaternary extension in southern Tibet–Field observations and Tectonic implications, *J. Geophys. Res.*, *91*(B14), 13,803–13,872, doi:10.1029/JB091iB14p13803.

Armijo, R., B. Meyer, G. C. P. King, A. Rigo, and D. Papanastassiou (1996), Quaternary evolution of the Corinth rift and its implications, *Geophys. J. Int.*, *126*, 11–53, doi:10.1111/j.1365-246X.1996.tb05264.x.

Armijo, R., B. Meyer, A. Hubert-Ferrari, and A. A. Barka (1999), Propagation of the North Anatolian fault into the northern Aegean: Timing and kinematics, *Geology*, *27*, 267–270, doi:10.1130/0091-7613(1999)027<0267:WPOTNA>2.3.CO;2.

Bemis, S. (2004), Neotectonic framework of the north-central Alaska Range foothills, M. S. thesis, Univ. of Alaska, Fairbanks.

Bemis, S. P., and W. K. Wallace (2007), Neotectonic framework of the north-central Alaska Range foothills, in *Tectonic Growth of a Collisional Continental Margin: Crustal Evolution of Southern Alaska*, edited by K. D. Ridgeway et al., *Geol. Soc. Am. Spec. Pap.*, *431*, 549–572.

Benson, L., R. Madole, W. Phillips, L. G. Thomas, and P. Kubik (2004), The probable importance of snow and sediment shielding on cosmogenic ages of north-central Colorado Pinedale and pre-Pinedale moraines, *Quat. Sci. Rev.*, *23*, 193–206, doi:10.1016/j.quascirev.2003.07.002.

Bevington, P. R., and D. K. Robinson (2002), *Data Reduction and Error Analysis for the Physical Sciences*, 336 pp., McGraw-Hill, Boston, Mass.

Bird, P. (1996), Computer simulations of Alaskan neotectonics, *Tectonics*, *15*, 225–256, doi:10.1029/95TC02426.

Bowman, D., G. King, and P. Tapponnier (2003), Slip partitioning by elastoplastic propagation of oblique slip at depth, *Science*, *300*(5622), 1121–1123, doi:10.1126/science.1082180.

Briner, J. P., D. S. Kaufman, A. Werner, M. Caffee, L. Levy, W. F. Manley, M. R. Kaplan, and R. C. Finkel (2002), Glacier readvance during the late glacial (Younger Dryas?) in the Ahklun Mountains, southwestern Alaska, *Geology*, *30*, 679–682, doi:10.1130/0091-7613(2002)030<0679:GRDTLG>2.0.CO;2.

Briner, J. P., D. S. Kaufman, W. F. Manley, R. C. Finkel, and M. W. Caffee (2005), Cosmogenic exposure dating of the late Pleistocene moraine stabilization in Alaska, *Geol. Soc. Am. Bull.*, *117*, 1108–1120, doi:10.1130/B25649.1.

Brown, E. T., R. Bendick, D. Bourles, V. Gaur, P. Molnar, G. M. Raisbeck, and F. Yiou (2002), Slip rates of the Karakorum Fault, Ladakh, India, determined using cosmic ray exposure dating of debris flows and moraines, *J. Geophys. Res.*, *107*(B9), 2192, doi:10.1029/2000JB000100.

Carlson, A. E. (2008), Why there was not a Younger Dryas-like event during the Penultimate Deglaciation, *Quat. Sci. Rev.*, *27*, 882–887, doi:10.1016/j.quascirev.2008.02.004.

Carver, G., G. Plafker, M. Metz, L. Cluff, B. Slemmons, E. Johnson, J. Roddick, and S. Sorenson (2004), Surface rupture on the Denali Fault interpreted from tree damage during the 1912 Delta Rive Mw 7.2–7.4 earthquake: Implications for the 2002 Denali Fault earthquake slip distribution, *Bull. Seismol. Soc. Am.*, *94*, S58–S71, doi:10.1785/0120040625.

Chevalier, M. L., F. J. Ryerson, P. Tapponnier, R. C. Finkel, J. Van Der Woerd, L. Haibing, and L. Qing (2005), Slip-rate measurements on the Karakorum Fault may imply secular variations in fault motion, *Science*, *307*, 411–414, doi:10.1126/science.1105466.

Cook, M. S., L. D. Keigwin, and C. A. Sancetta (2005), The deglaciation history of surface and intermediate water of the Bering Sea, *Deep Sea Res., Part II*, *52*, 2163–2173, doi:10.1016/j.dsr2.2005.07.004.

Crone, A. J., S. F. Personius, P. A. Craw, P. J. Haeussler, and L. A. Staft (2004), The Susitna Glacier Thrust Fault: Characteristics of surface ruptures on the fault that initiated the 2002 Denali Fault earthquake, *Bull. Seismol. Soc. Am.*, *94*, S5–S22, doi:10.1785/0120040619.

Daëron, M., L. Benedetti, P. Tapponnier, A. Sursock, and R. Finkel (2004), Constraints on the post ~25-ka slip rate of the Yammoûneh fault (Lebanon) using in situ cosmogenic 36Cl dating of offset limestone-clast fans, *Earth Planet. Sci. Lett.*, *227*, 105–119, doi:10.1016/j.epsl.2004.07.014.

DeMets, C., and T. H. Dixon (1999), New kinematic models for Pacific–North American motion from 3 Ma to present: I. Evidence for steady state motion and biases in the NUVEL-1A model, *Geophys. Res. Lett.*, *26*, 1921–1924, doi:10.1029/1999GL900405.

Eberhart-Phillips, D., et al. (2003), The 2002 Denali Fault earthquake, Alaska, *Science*, *300*, 1113–1118, doi:10.1126/science.1082703.

Engstrom, D. R., B. C. S. Hansen, and H. E. Wright Jr. (1990), A possible Younger Dryas record in southeastern Alaska, *Science*, *250*, 1383–1385, doi:10.1126/science.250.4986.1383.

Farber, D. L., G. S. Hancock, R. C. Finkel, and D. T. Rodbell (2005), 2005; The age and extent of tropical alpine glaciation in the Cordillera Blanca, Peru, *J. Quat. Sci.*, *20*, 759–776, doi:10.1002/jqs.994.

Friele, P. A., and J. J. Clague (2002), Younger Dryas readvance in Squamish river valley, southern Coast mountains, British Columbia, *Quat. Sci. Rev.*, *21*, 1925–1933, doi:10.1016/S0277-3791(02)00081-1.

Gaudemer, Y., P. Tapponnier, B. Meyer, G. Peltzer, S. M. Guo, Z. T. Chen, H. G. Dai, and I. Cifuentes (1995), Partitioning of crustal slip between linked, active faults in the eastern Qilian Shan, and evidence for a major seismic gap, the Tianzhu Gap, on the western Haiyuan Fault, Gansu, China, *Geophys. J. Int.*, *120*(3), 599–645, doi:10.1111/j.1365-246X.1995.tb01842.x.

Gosse, J. C., and F. M. Phillips (2001), Terrestrial in situ cosmogenic nuclides: Theory and application, *Quat. Sci. Rev.*, *20*(14), 1475–1560, doi:10.1016/S0277-3791(00)00171-2.

Gosse, J. C., E. B. Evenson, J. Klein, B. Lawn, and R. Middleton (1995a), Precise cosmogenic 10Be measurements in western North America: Support for a global Younger Dryas cooling event, *Geology*, *23*, 877–880, doi:10.1130/0091-7613(1995)023<0877:PCBMIW>2.3.CO;2.

Gosse, J. C., J. Klein, E. B. Evenson, B. Lawn, and R. Middleton (1995b), Beryllium-10 dating of the duration and retreat of the last Pinedale glacial sequence, *Science*, *268*, 1329–1333, doi:10.1126/science.268.5215.1329.

Haeussler, P., et al. (2004), Surface Rupture and Slip Distribution of the Denali and Totschunda Faults in the 3 November 2002 M 7.9 Earthquake, Alaska, *Bull. Seismol. Soc. Am.*, *94*, S23–S52, doi:10.1785/0120040626.

Henyey, T. L., and G. J. Wasserburg (1971), Heat flow near major strike-slip fault in California, *J. Geophys. Res.*, *76*, 7924–7946, doi:10.1029/JB076i032p07924.

Hickman, R. G., C. Craddock, and K. W. Sherwood (1977), Structural geology of the Nenana River segment of the Denali fault system, central Alaska Range, *Geol. Soc. Am. Bull.*, *88*, 1217–1230, doi:10.1130/0016-7606(1977)88<1217:SGOTNR>2.0.CO;2.

Hreinsdottir, S., J. Freymueller, H. Fletcher, C. Larsen, and R. Burgmann (2003), Coseismic slip distribution of the 2002 Mw7.9 Denali Fault earthquake, Alaska, determined from GPS measurements, *Geophys. Res. Lett.*, *30*(13), 1670, doi:10.1029/2003GL017447.

Hu, F. S., and A. Shemesh (2003), A biogenic-silica δ^{18}O record of climatic change during the last glacial–interglacial transition in southwestern Alaska, *Quat. Res.*, *59*, 379–385, doi:10.1016/S0033-5894(03)00056-5.

Hu, F. S., D. Kaufman, S. Yoneji, D. Nelson, A. Shemesh, Y. Huang, J. Tian, and T. Brown (2003), Cyclic variation and solar forcing of holocene climate in the Alaskan subarctic, *Science*, *301*, 1890–1893, doi:10.1126/science.1088568.

Hu, F. S., D. M. Nelson, G. H. Clarke, K. M. Ruhland, Y. Huang, D. S. Kaufman, and J. P. Smol (2006), Abrupt climatic events during the last glacial-interglacial transition in Alaska, *Geophys. Res. Lett.*, *33*, L18708, doi:10.1029/2006GL027261.

Hubert-Ferrari, A., A. Barka, E. Jacques, S. S. Nalbant, B. Meyer, R. Armijo, P. Tapponnier, and G. C. P. King (2000), Seismic hazard in the Marmara Sea region following the 17 August 1999 Izmit earthquake, *Nature*, *404*, 269–273, doi:10.1038/35005054.

Kaplan, K., D. Douglass, B. Singer, R. Ackert, and M. Caffee (2005), Cosmogenic nuclide chronology of pre-last glacial maximum moraines at Lago Buenos Aires, 46°S, Argentina, *Quat. Res.*, *63*, 301–315, doi:10.1016/j.yqres.2004.12.003.

King, G. C. P., R. S. Stein, and J. Lin (1994), Static stress changes and the triggering of earthquakes, *Bull. Seismol. Soc. Am.*, *84*, 935–953.

Kohl, C. P., and K. Nishiizumi (1992), Chemical Isolation of Quartz for Measurement of in situ-Produced Cosmogenic Nuclides, *Geochim. Cosmochim. Acta*, *56*(9), 3583–3587, doi:10.1016/0016-7037(92)90401-4.

Kovanen, D. J., and D. Easterbrook (2002), Timing and extent of Allerød and Younger Dryas age (ca 12,500–10,000 yr BP) oscillations of the Cordielleran Ice Sheet in the Fraser Lowland, western North America, *Quat. Res.*, *57*, 208–224, doi:10.1006/qres.2001.2307.

Lahr, J., and G. Plafker (1980), Holocene Pacific–North American plate interaction in southern Alaska: Implications for the Yakataga seismic gap, *Geology*, *8*, 483–486, doi:10.1130/0091-7613(1980)8<483:HPAPII>2.0.CO;2.

Lacourse, T. (2005), Late Quaternary dynamics of forest vegetation on northern Vancouver Island, British Columbia, Canada, *Quat. Sci. Rev.*, *24*, 105–121, doi:10.1016/j.quascirev.2004.05.008.

Lakeman, T. R., J. L. Clague, and B. Menounos (2008), Advance of Alpine glaciers during final retreat of the Cordilleran ice sheet in the Finlay River area, northern British Columbia, Canada, *Quat. Res.*, *69*, 188–200, doi:10.1016/j.yqres.2008.01.002.

Lal, D. (1991), Cosmic ray labeling of erosion surfaces: In situ production rates and erosion models, *Earth Planet. Sci. Lett.*, *104*, 424–439, doi:10.1016/0012-821X(91)90220-C.

Lasserre, C., et al. (1999), Postglacial left slip rate and past occurrence of M > 8 earthquakes on the western Haiyuan fault, Gansu, China, *J. Geophys. Res.*, *104*(B8), 17,633–17,652.

Lasserre, C., Y. Gaudemer, P. Tapponnier, A. S. Mériaux, J. Van der Woerd, D. Y. Yuan, F. J. Ryerson, R. C. Finkel, and M. W. Caffee (2002), Fast late Pleistocene slip rate on the Leng Long Ling segment of the Haiyuan fault, Qinghai, China, *J. Geophys. Res.*, *107*(B11), 2276, doi:10.1029/2000JB000060.

Leloup, P. H., T. M. Harrison, F. J. Ryerson, W. Chen, L. Qi, P. Tapponnier, and R. Lacassin (1993), Structural, petrological and thermal evolution of a Tertiary ductile strike-slip shear zone, Diancang Shan, Yunnan, *J. Geophys. Res.*, *98*(B4), 6715–6743, doi:10.1029/92JB02791.

Lesh, M. E., and K. D. Ridgway (2007), Geomorphic evidence of active transpressional deformation in the Tanana foreland basin, south-central Alaska, in *Tectonic Growth of a Collisional Continental Margin: Crustal Evolution of Southern Alaska*, edited by K. D. Ridgway et al., *Geol. Soc. Am. Spec. Pap.*, *431*, 573–592.

Matmon, A., D. Schwartz, P. Haeussler, R. Finkel, J. Lienkaemper, H. D. Stenner, and T. E. Dawson (2006), Denali fault slip rates and Holocene–late Pleistocene kinematics of central Alaska, *Geology*, *34*(8), 645–648, doi:10.1130/G22361.1.

McElhinny, M. W., and W. E. Senanayake (1982), Variations in the geomagnetic dipole. I - The past 50,000 years, *J. Geomagn. Geoelectr.*, *34*, 39.

Mériaux, A.-S., F. J. Ryerson, P. Tapponnier, J. Van der Woerd, R. C. Finkel, X. Xu, Z. Xu, and M. W. Caffee (2004a), Rapid slip along the central Altyn Tagh Fault: Morphochronologic evidence from Cherchen He and Sulamu Tagh, *J. Geophys. Res.*, *109*, B06401, doi:10.1029/2003JB002558.

Mériaux, A.-S., K. Sieh, C. Rubin, F. J. Ryerson, R. C. Finkel, A. Meltzner, and M. Taylor (2004b), Kinematics of the southern Alaska constrained by westward-decreasing post-glacial slip-rates on the Denali Fault, Alaska, *Eos Trans. AGU*, *85*(47), Fall Meet. Suppl., Abstract G13C–07.

Mériaux, A.-S., et al. (2005), The Aksay segment of the northern Altyn Tagh fault: Tectonic geomorphology, landscape evolution, and Holocene slip rate, *J. Geophys. Res.*, *110*, B04404, doi:10.1029/2004JB003210.

Meyer, B., P. Tapponnier, L. Bourjot, F. Metivier, Y. Gaudemer, G. Peltzer, G. Shunmin, and C. Zhitai (1998), Crustal thickening in Gansu-Qinghai, lithospheric mantle subduction, and oblique, strike-slip controlled growth of the Tibet plateau, *Geophys. J. Int.*, *135*(1), 1–47, doi:10.1046/j.1365-246X.1998.00567.x.

Nishiizumi, K., E. L. Winterer, C. P. Kohl, J. Klein, R. Middleton, D. Lal, and J. R. Arnold (1989), Cosmic ray production rates of 10Be and 26Al in quartz from glacially polished rocks, *J. Geophys. Res.*, *94*, 17,907–17,915, doi:10.1029/JB094iB12p17907.

Nishiizumi, K., M. Imamura, M. W. Caffee, J. R. Southon, and R. C. Finkel (2007), c, J. McAninch, Absolute calibration of 10Be AMS standards, *Nucl. Instrum. Methods Phys. Res., Sect. B*, *258*, 403–413, doi:10.1016/j.nimb.2007.01.297.

Ohno, M., and Y. Hamano (1992), Geomagnetic poles over the past 10,000 years, *Geophys. Res. Lett.*, *19*(16), 1715–1718, doi:10.1029/92GL01576.

Page, R. A., N. N. Biswas, J. Lahr, and H. Pulpan (1991), Seismicity of continental Alaska, in *Neotectonics of North America, Decade Map*, vol. 1, edited by D. B. Slemmons et al., pp. 47–68, Geol. Soc. of Am., Boulder, Colo.

Page, R. A., G. Plafker, and H. Pulpan (1995), Block rotation in east-central Alaska: A framework for evaluating earthquake potential?, *Geology*, *23*, 629–632, doi:10.1130/0091-7613(1995)023<0629:BRIECA>2.3.CO;2.

Peltzer, G., and P. Tapponnier (1988), Formation and evolution of strike-slip faults, rifts, and basins during the India-Asia collision - An experimental approach, *J. Geophys. Res.*, *93*, 15,085–15,117, doi:10.1029/JB093iB12p15085.

Plafker, G., and H. Berg (1994), An overview of the geology and tectonic evolution of Alaska, in *The Geology of Alaska*, edited by H. Berg, pp. 989–1021, Geol. Soc. of Am., Boulder, Colo.

Ratchkovski, N. A., S. Wiermer, and R. A. Hansen (2004), Seismotectonics of the central Denali Fault, Alaska, and the 2002 Denali Fault earthquake sequence, *Bull. Seismol. Soc. Am.*, *94*, S156–S174, doi:10.1785/0120040621.

Richter, D. H., and N. A. Matson (1971), Quaternary faulting in the eastern Alaska range, *Geol. Soc. Am. Bull.*, *82*, 1529–1539, doi:10.1130/0016-7606(1971)82[1529:QFITEA]2.0.CO;2.

Schildgen, T. F., W. M. Phillips, and R. S. Purves (2005), Simulation of snow shielding corrections for cosmogenic nuclide surface exposure studies, *Geomorphology*, *64*, 67–85, doi:10.1016/j.geomorph.2004.05.003.

Schwartz, D. P. (2003), Paleoearthquakes on the Denali-Totschunda Fault system: Preliminary observations of slip and timing, *Eos Trans. AGU*, *84*(46), Fall Meet. Suppl., Abstract S11B–03.

Sieh, K. (1981), A review of geological evidence for recurrence times of large earthquakes, in *Earthquake Prediction–An International Review, Maurice Ewing Ser.*, vol. 4, edited by D. W. Simpson and P. G. Richards, pp. 181–207, AGU, Washington, D. C.

St. Amand, P. (1957), Geological and geophysical synthesis of the tectonics of portions of British Columbia, the Yukon territory, and Alaska, *Geol. Soc. Am. Bull.*, *68*, 1343–1370, doi:10.1130/0016-7606(1957)68[1343:GAGSOT]2.0.CO;2.

Stein, R. S., G. C. P. King, and J. Lin (1992), Change in failure stress on the southern San Andreas fault system caused by the 1992 Magnitude = 7.4 Landers earthquake, *Science*, *258*, 1328–1332, doi:10.1126/science.258.5086.1328.

Stone, J. O. (2000), Air pressure and cosmogenic isotope production, *J. Geophys. Res.*, *105*, 23,753–23,759, doi:10.1029/2000JB900181.

Stout, J., and C. Chase (1980), Plate kinematics of he Denali fault system, *Can. J. Earth Sci.*, *17*, 1527–1537.

Stout, J. H., J. B. Brady, F. Weber, and R. A. Page (1973), Evidence for Quaternary movement on the McKinley strand of the Denali fault in the Delta River area, Alaska, *Geol. Soc. Am. Bull.*, *84*, 939–948, doi:10.1130/0016-7606(1973)84<939:EFQMOT>2.0.CO;2.

Taylor, M., S. LePrince, J. P. Avouac, and K. Sieh (2008), Detecting coseismic displacements in glaciated regions: An example from the Great November 2002 Denali Earthquake using SPOT horizontal offsets, *Earth Planet. Sci. Lett.*, *270*, 209–220, doi:10.1016/j.epsl.2008.03.028.

Van der Woerd, J., F. J. Ryerson, P. Tapponnier, Y. Gaudemer, R. Finkel, A. S. Meriaux, M. Caffee, G. G. Zhao, and Q. L. He (1998), Holocene left-slip rate determined by cosmogenic surface dating on the Xidatan segment of the Kunlun fault (Qinghai, China), *Geology*, *26*(8), 695–698, doi:10.1130/0091-7613(1998)026<0695:HLSRDB>2.3.CO;2.

Van der Woerd, J., P. Tapponnier, F. J. Ryerson, A. S. Meriaux, B. Meyer, Y. Gaudemer, R. C. Finkel, M. W. Caffee, G. G. Zhao, and Z. Q. Xu (2002), Uniform postglacial slip-rate along the central 600 km of the Kunlun Fault (Tibet), from Al-26, Be-10, and C-14 dating of riser offsets, and climatic origin of the regional morphology, *Geophys. J. Int.*, *148*(3), 356–388, doi:10.1046/j.1365-246x.2002.01556.x.

Wright, T., Z. Lu, and C. Wicks (2004), Constraining the slip distribution and fault geometry of the Mw7.9, 2 November 2002, Denali Fault earthquake with interferometric synthetic aperture radar and global positioning system data, *Bull. Seismol. Soc. Am.*, *94*(6B), S175–S189, doi:10.1785/0120040623.

R. C. Finkel, Earth and Planetary Science Department, University of California, Berkeley, 307 McCone Hall, Berkeley, CA 94720-4767, USA.

A. J. Meltzner and K. Sieh, Division of Geologic and Planetary Science, California Institute of Technology, Pasadena, CA 91125, USA.

A.-S. Mériaux, School of Geography, Politics and Sociology, University of Newcastle, Claremont Road, Newcastle Upon Tyne NE1 7RU, UK. (a.s.meriaux@ncl.ac.uk)

C. M. Rubin, Department of Geological Sciences, Central Washington University, Ellensburg, WA 98926, USA.

F. J. Ryerson, Institute of Geophysics and Planetary Physics, Lawrence Livermore National Laboratory, Livermore, CA 94550, USA.

M. H. Taylor, Department of Geology, University of Kansas, 114 Lindley Hall, Lawrence, KS 66045, USA.